ULTRAHIGH-RESOLUTION PARAGENESIS OF THE CAMBRIAN-AGE MT. SIMON SANDSTONE AT A BURIAL DEPTH OF 1.8-2.1 KM, ILLINOIS BASIN, USA

BY

PHILIP ALEXANDER MILLER

THESIS

Submitted in partial fulfillment of the requirements
for the degree of Master of Science in Geology
in the Graduate College of the
University of Illinois at Urbana-Champaign, 2011

Urbana, Illinois

Adviser:

Associate Professor Bruce W. Fouke

ABSTRACT

A multidisciplinary study utilizing new ultrahigh-resolution microscopy techniques has been undertaken to reconstruct the paragenesis of Cambrian-age Mt. Simon Sandstone quartz arenites buried at 1.8-2.1 km within the Illinois Basin. Results have yielded valuable new insight into the evolution of this important subsurface reservoir and provided the depositional and diagenetic history required to enhance carbon capture and storage (CCS) strategies within early Paleozoic strata of the Illinois Basin. Petrographic analyses of the host quartz arenite Mt. Simon Sandstone lithologies, coupled with wireline log data and formation on Sr-isotope water geochemistry, have permitted the construction and interpretation of a complex sequence of paragenetic events.

Core samples were collected from the Illinois Basin-Decatur Project CCS injection well. The 1.8-2.1 km interval of the well was sampled using a Schlumberger mechanical sidewall coring tool, a Modular Formation Dynamics Tester (MDT) and openhole wireline tools. Sidewall cores were extracted from seven stratigraphic horizons (1783 m [5851 ft], 1785 m [5856 ft], 1829 m [6000 ft], 2061 m [6763 ft], 2085 m [6841 ft], 2147 m [7045 ft] and 2148 m [7048 ft]), which have been grouped into lower (2148 - 2061m [7048 - 6763 ft]) and upper (1829 - 1783 m [6000 ft - 5851 ft]) stratigraphic intervals. Polished thin sections were analyzed under plane-light (PL), polarized-light using a Zeiss Axiovert 200M Inverted Fluorescence Microscope (optical resolution of 250 nm), in coordination with analyses on a stand-alone cathodoluminescence-light (CL) stage. The combination of core sample microscopy and wireline log data indicate the lower sampling interval (2.0 - 2.1 km) is a clean quartz arenite with high porosity and permeability. Conversely, the upper sampling interval (1.8 - 1.9 km) exhibit significantly greater clay content and the formation of quartz cement overgrowths that have served to reduce primary porosity and permeability. This represents an up-section depositional shift from distal to more proximal positions within deltaic alluvial fans in arid high-relief terrestrial depositional environments during the Cambrian. Furthermore, the microscopy has been used to document a multistage paragenetic sequence of grain contact suturing during an early compaction event, followed by iron oxide (hematite and goethite) and clay cement precipitation. These were followed by two events of syntaxial, euhedral quartz cement overgrowths and a final ensuing event of iron oxide cements on the quartz cement overgrowths. Comparison of this paragenetic sequence with results

from previous studies of the Mt. Simon Sandstone and other early Paleozoic strata in the Midwest, suggest that the quartz overgrowth cements were formed at a maximum burial depth of no more than 2.4 km and maximum burial temperatures greater than 100°C during the late-Paleozoic to early-Mesozoic (Fishman 1997). The modern formation waters have $^{87}Sr/^{86}Sr$ analyses that more radiogenic than younger Paleozoic strata within the Illinois Basin, and reconstructed values for Cambrian seawater (Stueber et al. 1987; Veizer et al. 1999), suggesting potential sources of radiogenic Sr from internal Mt. Simon Sandstone sands and shales or the Precambrian basement. These results indicate that, due to multiple events of heterogeneous subsurface fluid flow and associated diagenesis, the Mt. Simon Sandstone experienced low to moderate porosity and permeability occlusion during its burial and uplift history within the Illinois Basin.

ACKNOWLEDGMENTS

This project could not have been completed without the help of many individuals. I would like to first thank my adviser, Dr. Bruce W. Fouke, for his countless hours of guidance, as well as sharing his knowledge and opportunities with me throughout the years. It truly made my experience at the University of Illinois at Urbana-Champaign (UIUC) unforgettable. I would also like to thank the members of the Fouke Lab Group for their support and assistance. Thanks to Dr. Mayandi Sivaguru at the Institute for Genomic Biology (IGB) Core Facilities and Dr. Thomas M. Johnson at the Geology Department at UIUC. This project would not have been accomplished without assistance from the IGB Energy Biosciences Institute (EBI), Dr. Brenda Beitler Bowen at Purdue University, Schlumberger Limited, Illinois State Geological Survey (ISGS) and Midwest Geological Sequestration Consortium (MGSC). And finally, I would like to thank my wife, parents, brother and family-in-law for their continual support and love.

TABLE OF CONTENTS

CHAPTER 1
INTRODUCTION

Deep subsurface sedimentary rock reservoirs commonly associated with hydrocarbon entrapment are now important targets for large-scale carbon capture, transport and storage (CCS) projects (Morse and Leetaru 2003; Leetaru et al. 2009; DOE 2010). The high porosity and permeability characteristic of these CCS reservoirs is strongly influenced by both depositional and post-depositional (diagenetic) alternation process. The most significant diagenetic processes include compaction, tectonically-driven fluid migration, and the resulting precipitation or dissolution of minerals during subsurface water-rock interaction (Bethke 1985; Leach and Rowan 1986; Oliver 1986; Fishman 1997). One common diagenetic product of these processes is the precipitation of cements within pore space, which serves to reduce or occlude primary porosity. Reconstruction of the timing, source and composition of the burial brines that precipitate these cements provide vitally important information for the development of effective CCS approaches (Bao et al. 2009; Leetaru et al. 2009; Bowen et al. 2011).

The intracratonic Illinois Basin contains several subsurface Paleozoic sandstone and limestone reservoirs that are hydrologically sealed by widespread shale deposits and are now viable CCS reservoir targets (Buschbach and Kolata 1991; Goetz et al. 1992; McBride et al. 2003; Leetaru et al. 2009). Among these, the thick (153-610 m [500-2000 ft]) regionally continuous Cambrian-age Mt. Simon Sandstone is potentially the most capable of holding large volumes of injected supercritical CO_2 (Bethke 1986; Fishman 1997; Rowan and de Marsily 2001; Leetaru et al. 2009; DOE 2010; Kolata 2010). The Mt. Simon Sandstone, which directly overlies the Precambrian crystalline basement of the Illinois Basin, experienced increasing subsidence and burial throughout the Paleozoic, having reached a maximum burial depth of 2.4 km and temperature of 100°C in the early Mesozoic (Rowan et al. 2002; Makowitz et al. 2006).

The early Paleozoic section of the Illinois Basin, including the Mt. Simon Sandstone, may have experienced multiple events of regionally subsurface fluid flow. Tectonic events are suggested to influence and cause such paleofluid flows (Bethke et al. 1984; Bethke 1986; Bethke and Marshak 1990; Bethke et al. 1991; Stueber and Walter 1991). However, the origin of the brines associated with these water-rock interaction events remain a topic of debate, particularly

because the Illinois Basin lacks widespread evaporite deposits from which the brine salts could have been derived (Clayton et al. 1966). Shale-membrane filtration is one possible source (Bredehoeft et al. 1963). However, this is not likely because the Illinois Basin was never overpressured during subsidence due to the slow burial rates, low volume of shale deposition, and the laterally continuous basal aquifer (Bethke 1986). The modeling of modern formation water chemistry suggests that the Illinois Basin brines were instead derived from evaporated seawater, which was then modified via subsurface water-rock interactions and later partially mixed with recharging meteoric groundwater (Walter et al. 1990; Stueber and Walter 1991; Stueber et al. 1993).

Given these uncertainties, an accurate understanding of the geologic history of the Mt. Simon Sandstone is especially important to guide the development of CCS strategies (Leetaru et al. 2009; Bowen et al. 2011). Therefore, the present study has been undertaken in order to reconstruct a detailed ultrahigh-resolution paragenetic history of the Mt. Simon Formation from core samples. This has been accomplished by analyzing samples from the 1.8-2.1 km depth interval of the Mt. Simon Sandstone with multiple cutting-edge techniques, which include ultrahigh-resolution plane-polarized light and cathodoluminescence-light petrography, electrical wireline log data and strontium-isotope analyses of formation water samples collected from the flagship CCS Illinois Basin – Decatur Project. The integration of these data sets has permitted reconstruction of the timing, temperature, depth and source of the diagenetic burial brines that caused subsurface diagenetic alteration of the Mt. Simon Sandstone CCS reservoir. These results will also establish the required contextual geological framework for ongoing and future studies of the deep subsurface microbial biosphere inhabiting these reservoirs.

CHAPTER 2
GEOLOGICAL SETTING

The Illinois Basin is an oval-shaped depression that covers 284,899 km^2 of the U.S. Midcontinent (Kolata and Nelson 2010; Fig. 1). The deposition and structure of the Paleozoic sequence of terrestrial to marine siliciclastics (primarily sandstones and shales) and marine carbonates has been strongly influenced by multiple episodes of tectonic deformation beginning in the late Precambrian and continuing throughout the Phanerozoic (Buschbach and Kolata 1991; McBride et al. 2003). Five major tectonic events have been identified, including: (1) Precambrian to Late Cambrian subsidence that formed a proto-Illinois Basin and initiated deposition of the Cambrian Mt. Simon Sandstone; (2) Late Precambrian to Middle Cambrian rifting (New Madrid Rift System) that formed the Reelfoot Rift and Rough Creek Graben in the south and strongly controlled basin geometry and subsidence; (3) continued early Paleozoic subsidence of the rift system resulting in a southwest plunging trough; (4) Pennsylvanian to late Cretaceous uplift and erosion of the Pascola arch, which formed perpendicular to the Reelfoot Rift created the modernday spoon-shaped depression; and (5) Late Cretaceous to Tertiary subsidence of the Reelfoot Rift resulting in the deposition of the Mississippi embayment deposits of the Gulf Coastal Plain (Kolata and Nelson 1991; Seyler and Cluff 1991; McBride et al. 2003; Kolata and Nelson 2010). These tectonic events occurred periodically throughout the Paleozoic. This has produced multiple large-scale subsurface hydrologic exchanges, the most recent of which occurred in the Pennsylvanian-Permian time (~260 Ma) period associated with the Alleghanian and Ouchita orogenies (Duffin et al. 1989; Bethke and Marshak 1990; Buschbach and Kolata 1991; Kolata and Nelson 1991; Fishman 1997). The Illinois Basin reached a maximum burial depth of ~2.4 km and temperatures of ~100˚C as depicted by burial curves and thermal history modeling, and homogenization temperatures of 100-130˚C from fluid inclusion data (Fishman 1997; Rowan et al. 2002; Makowitz et al. 2006). This history of tectonic and thermal subsidence has produced well-sealed Paleozoic sandstone, limestone and shale deposits that form excellent reservoirs for both hydrocarbon entrapment and regional CO_2 sequestration (Leetaru et al. 2009; DOE 2010).

The Cambrian-age Mt. Simon Sandstone unconformably overlies a weathered Precambrian granite and rhyolite basement and comprises the lower part of an early Paleozoic

sedimentary sequence know as the Sauk sequence (Sloss 1963; Houseknecht and Ethridge 1978; Kolata 1991; Kolata 2010; Fig. 2). The Mt. Simon Sandstone is heterogeneous in composition, consisting of six variable lithofacies that include: 1) cobble conglomerate, 2) stratified gravel conglomerate, 3) poorly-sorted sandstone (most common), 4) well-sorted sandstone, 5) interstratified sandstone and shale, and 6) shale (Driese et al. 1981; Fishman 1997; Leetaru and McBride 2009; Bowen et al. 2011). The lower section of the Mt. Simon Sandstone is dominated by the cobble and stratified gravel conglomerate lithofacies, suggesting alluvial fan and braided river depositional environments (Houseknecht and Ethridge 1978; Leetaru and McBride 2009; Bowen et al. 2011). The middle and upper sections of the Mt. Simon Sandstone are composed of the tidal-flat, shallow marine subtidal or marginal marine environment represented by the presence of marine trace fossils (*Skolithos, Planolites, Arenicolites, Cruziana, Teichichnus*) with interstratified sandstones and shale (Driese et al. 1981; Duffin et al. 1989). The shale lithofacies occur in thin beds (~5 mm thick), and contain no trace fossils (*Planolites*), suggesting deposition within a marine lagoon environment, which may have been anoxic because of restricted circulation of water (Bowen et al. 2011).

The Mt. Simon Sandstone reaches a maximum thickness of 914 meters (3000 ft) in east-central Illinois and thins towards the edges of the basin (Buschbach 1975; Kolata 2010). The regional thickness is dependent on tectonic and thermal subsidence, but locally dependent on the topography of the Precambrian basement that in some locations has a topographic relief greater than 590 m (1800 ft), influencing both the thickness and presence of the Mt. Simon Sandstone (Leetaru and McBride 2009). Beneath Decatur, Illinois (39°51′6″N 88°56′39″W) in east-central Illinois, the Mt. Simon Sandstone Formation is 494 m (1620 ft) thick, with the formation top at a depth of 1690 m (5550 ft) and the base at 1196 m (3924 ft). Porosity can be as high as 25% and permeability can reach 1000mD (Leetaru et al. 2009). These depositional and diagenetic heterogeneities play a major role in determining the reservoir properties and are also directly related to the formational fluid flow paths (Bowen et al. 2011).

CHAPTER 3
MATERIALS AND METHODS

3.1 Formation Water Collection

Mt. Simon Sandstone formation water was collected by Schlumberger Limited, a major corporation providing oilfield services, for the Illinois State Geological Survey (ISGS) with the Schlumberger Modular Formation Dynamics Tester (MDT; http://www.slb.com) attached with the recently developed Quicksilver Probe (Fig. 3). The Quicksilver Probe is a down-hole tool designed for "low contaimination" sampling of subsurface oil and formation water. This is accomplished with a pump design incorporating inner and outer probe rings for active suction sampling. The outer ring draws contaminated fluids (e.g. drilling mud filtrates, oils, etc.) to the perimeter of the probe where it is pumped into a separate flowline, while the center ring samples formation waters from deeper within the surrounding rock formation. The inner and outer ring flowlines are monitored in real-time for resistivity measurements and real-time adjustments can be made as needed to the pumping rate from the surface for quality control of the formation fluid sample. When the resistivity measurements, which act as a tracer for drilling fluid contamination, reaches 0.02 ohms the fluid contamination is considered to be low enough for the water sample to be collected within ethanol-cleaned MDT sample containers (Phelps and Fredrickson 2002). Additional tracers and procedures that are presented by Phelps and Fredrickson (2002) were thoroughly considered, but ultimately abandoned due to high expense.

The MDT with Quicksilver probe was initially lowered into the well bore and pumped at multiple positions throughout the Mt. Simon Sandstone to indentify horizons at which rock formation porosity and permeability was high enough to sustain appreciable flow for sample collection. Based on these well bore tests, formation water was collected at the following horizons: (1) 10.4 L at 1790 m (5872 ft); (2) 10.4 L at 2062 m (6764 ft); (3) 3.79 L at 2084.8 m (6840 ft); and (4) 3.79 L at 2147 m (7045 ft) (Fig. 4). Once the water was collected from the specified locations, the MDT was taken out of the borehole and transferred to the Schlumberger MDT trailer. The MDT sample containers were attached to a small, ethanol cleaned Christmas tree, a device consisting of a small set of valves and a pressure gauge that is used to slowly release the pressure from the MDT containers. As the pressure was slowly released, the formation fluid was transferred directly from the MDT containers through the tree and tygon

tubing into autoclaved 1L Nalgene bottles with gloved hands. Once the water samples were collected in the Nalgene bottles, they were immediately wrapped in Parafilm and placed in a cooler at 4˚C, and transported back to University of Illinois at Urbana-Champaign and were stored in the dark in a 4˚C cold room for up to 60 days, before the Sr lab analyses were performed.

3.2 Rock Collection/Petrography

A suite of 51 side-wall cores (2.3 cm x 5 cm) were collected by Schlumberger for the ISGS with the Schlumberger mechanical sidewall coring tool (MSCT; http://www.slb.com). This hollow rotary drill cuts laterally into the rock formation from inside the borehole to extract *in situ* bedrock samples (Fig. 3). From this sample suite, a total of 7 cores were chosen for analysis based on their stratigraphic proximity to the 4 specific horizons from which formation water was sampled (Fig. 4). These included 1783 m (5851 ft), 1785 m (5856 ft), 1829 m (6000 ft), 2061 m (6763 ft), 2085 m (6841 ft), 2147 m (7045 ft), and 2148 m (7048 ft). A total of 11 standard-sized, 30 μm thick, polished uncovered thin sections were prepared from the chosen sidewall cores (Fig. 4). Thin sections were prepared by Wagner Petrographic (http://www.wagnerpetrophic.com). Each thin section was analyzed under plane-light (PL) and polarized light using an Axiovert 200M Fluorescent Microscope with Apotome (Zeiss, Obercochen, Germany) operated by Axiovision software, allowing for ultrahigh resolution imaging and microscopy (125-200 nanometer working resolution). Images were collected with an AxioCam MRc5 color camera and an AxioCam MRm high resolution camera and analyzed for grain size and shape using the Axiovision software. All of the sidewall core lithologies were described using the Williams et al. (1982) siliciclastic sedimentary rock classificiation scheme.

The samples were also investigated under cathodoluminescence-light (CL) microscopy using a Relion Industries Cold Cathodoluminescence Stage. Images were captured using a thermoelectrically cooled color video camera (Fouke and Rakovan 2001) using Final Cut Express software. The CL conditions for the imaging were completed with 8 second shutter duration with a beam voltage of 7.8 kilovolts (kV). CL emissions are generated by bombarding a thin section sample with an energetic electron beam, with the resulting light wavelengths indicative of mineral composition and distribution (Marshall 1988). The CL images are then used to document depositional and diagenetic processes, such as growth zoning and secondary quartz

emplacement within fractures, and interpret the diagenetic history (Sippel 1968; Goetze et al. 1999). Minerals to note in the Mt. Simon Sandstone are feldspars and quartz. Feldspars exhibit a CL emission color of greenish-yellow or red in response to Mn^{2+}, Fe^{2+}, Fe^{3+}, Cu^{2+}, rare earth elements (REE) (Mariano et al. 1973; Marshall 1988; Götze et al. 1999). The Mt. Simon Sandstone has a dominant bright blue color, which is a response to the activating ion Ti^{4+} (Marshall 1988). In a variety of, cathodoluminescence studies, quartz has been recorded emitting a dull blue, as seen in the Mt. Simon Sandstone, dull red, yellow, orange, brown, gray and purple (Marshall 1988; Goetze et al. 1999; Götze et al. 2001). The variation in colors in quartz is not well understood, but has been attributed to lattice defects and rare substitutions of the silicon atoms with Al^{3+} in quartz and to a lesser extent Ga^{3+}, Fe^{3+}, Ge^{4+}, Ti^{4+} and P^{5+} (Marshall 1988; Götze et al. 2001).

In addition, a scanning electron microscope (SEM) analysis was completed on a Mt. Simon Sandstone samples from a depth of 1961 m (6433 ft) using a Philips XL30 Field-Emission Environmental Scanning Electron Microscope (ESEM-FEG) with a 2 nm ultimate resolution. A solid rock sample was prepared through critical point drying and coating with a gold/palladium target with spare gold and platinum by a Denton Desk II TSC turbo-pumped sputter coater, with rotating/tilting specimen holder and film thickness monitor. The ESEM-FEG also collected energy-dispersive spectroscopy (EDS) data. These analyses were used to visualize clay content within the sample as well as the elemental composition of the clays.

3.3 Petrophysical Data Collection

The sidewall cores were used in conjunction with a suite of openhole wireline tools. A wireline tool is a cylindrical device that consists of one to multiple tools that each collects specific data, such as porosity and permeability. Wireline tools are lowered to the base of the well and slowly pulled to the surface, while collecting data. Wireline logs provide a comprehensive analysis of reservoir characteristics by indicating different parameters, such as porosity, permeability and lithologies. The tools used to create these logs were the gamma ray, neutron porosity, and nuclear magnetic resonance (NMR). The gamma ray log measurements recorded the amount of naturally occurring radioactivity within a deposit from various radioactive elements, such as potassium, uranium and thorium, and are presented in a relative scale that ranges from 0 to 200. The neutron porosity log is based on the effect of a formation on

neutrons emitted by a source. Hydrogen has the largest effect on slowing or capturing neutrons and because hydrogen is mainly in pore fluids, the porosity can be inferred. The nuclear magnetic resonance (NMR) tool measures the pore size distribution, and is used in the Schlumberger-Doll Research permeability (SDR Perm) equation to estimate permeability (Fig. 4; https://www.slb.com).

3.4 Strontium Isotopic Analysis

Strontium (Sr) analyses were completed by in the Department of Geology at University of Illinois at Urbana-Champaign on the formation water from the MDT. The Sr purification followed standard procedures using Sr-spec resin in 0.2 mL Teflon columns and nitric acid media. The Sr-isotopes were analyzed using a Nu Plasma HR (MC-ICP-MS) (multicollector inductively-coupled-plasma mass spectrometer) with consistent plasma parameters of: (1) coolant gas: 13L/min; (2) auxiliary gas: 0.9L/min; (3) RF power: 1300W. The solution samples, at ~100 ng/mL Sr, were introducted into a DSN-100 desolvating nebulizer.

Along with Sr isotopes, ^{85}Rb and ^{83}Kr signals were measured and using natural ratios and the mass bias of the instrument determined during each measurement, isobaric interferences of ^{87}Rb, ^{84}Kr and ^{86}Kr were subtracted from the Sr peaks. $^{87}Sr/^{86}Sr$ was calculated based on the measured $^{86}Sr/^{88}Sr$ assuming an exponential mass bias from a true ratio of 0.1194. The NBS 987 standard and an in house coral standard were run every 5 and 10 samples, respectively. The running laboratory average for NBS 987 over the time period of this study was 0.710267 +/- 0.000018 and produced an analytical error of about ±0.00003. Veizer et al. (1999) reported a NBS 987 of 0.710240. Therefore, a constant of 0.000027 has been subtracted from the data measured in this study for a direct comparison to Veizer et al. (1999).

CHAPTER 4
RESULTS

4.1 Sedimentology and Stratigraphy

The lithologies comprising the Mt. Simon Sandstone were analyzed from sidewall core samples collected at two subsurface stratigraphic horizons, which include (Fig. 4): (1) a Lower Stratigraphic Interval at 2148 m to 2061m (7048 ft – 6763 ft); and (2) an Upper Stratigraphic Interval between 1829m to 1783 m (6000 ft – 5851 ft). Lithologic analyses of the sidewall core samples from these two intervals have been synthesized into a single comprehensive paragenetic sequence for the Mt. Simon Sandstone (Fig. 5)

The Lower Stratigraphic Interval (Fig. 4, 6) is composed of fine to medium grained quartz arenites with abundant iron oxide cements, which have been identified through spectral data to be hematite and goethite (Bowen et al. 2011), and relatively small abundance of quartz cement overgrowths (Fig. 4). The lower two quartz arenite samples (2148 m [7048 ft] and 2147 m [7045 ft]) are composed of sub-rounded, moderately well-sorted, sand-sized (70 – 800 μm) quartz grains coated with dark red iron oxide cement rims (Fig. 6, 4). Quartz cement overgrowths at these depths are thin and poorly developed (Fig. 6). In addition, unique groupings of concentric conchoidal fractures were observed exclusively within the sample from 2148 m (7045 ft; Fig. 6). Based on discussion with Schlumberger technicians, these fractures are interpreted to be an artifact of the mechanical sidewall coring tool, which drills into the rock formation from inside the borehole and thus can cause fracturing. The sample from 2085 m (6841 ft) contains sub-rounded, moderately well-sorted sand-sized (~100 – 700 μm in diameter) quartz grains with dark red iron oxide cement rims. Sutured grain contacts are present that clearly pre-date the precipitation of quartz cement overgrowths within this horizon (Fig. 7, 4). Samples from 2061 m (6763 ft) are composed of sub-angular, moderately well-sorted, and sand-sized (~80 – 350 μm) quartz grains. Dark red iron oxide cement rims coat the quartz grains and occur at the sutured grain contacts, while quartz overgrowth cements remain poorly developed and relatively rare (Fig. 7, 4).

The Upper Stratigraphic Interval (Fig. 4) is composed of moderately well to well-sorted, medium to coarse grained quartz arenite in which dark red iron oxide cements are coated with

thicker, more abundant and well-developed quartz overgrowth cements, compared to the Lower Stratigraphic Interval (Fig. 4, 8). These are in turn encrusted by later dark red iron oxide cement (Fig. 8). The sample from 1829 m (6000 ft) consists of well-rounded and well sorted quartz grains (~100 – 600 µm in diameter) (Fig. 4). The outer surfaces of these quartz grains are coated with an iron oxide-quartz-iron oxide cement sequence (Fig. 8), where the quartz cement overgrowths have served to significantly reduce the porosity and permeability of the host quartz arenite. The quartz arenite sample from 1785 m (5856 ft) is composed of well-sorted, angular to sub-rounded quartz grains (~60 – 100 µm) that are interbedded with mud-sized grains and micas (Fig. 9). In these intercalated fine grained deposits, there are no easily visible quartz cement overgrowths and little porosity due to the increased fine matrix content (Fig. 9, 4). The sample from 1783 m (5851 ft) consists of moderately well-sorted, sub-angular, sand-sized (~60 – 150 µm) quartz grains with a dark red iron oxide cement rim with sutured quartz grain contacts (Fig. 9). Quartz overgrowth cements are again abundant and significantly occlude the porosity and permeability in this horizon (Fig. 9, 4).

4.2 Petrophysical Analyses

Data from Schlumberger wireline logs (gamma, porosity and permeability; Fig. 10) were used to contextualize the bulk rock properties of each sidewall core sampled. The Lower Stratigraphic Interval at 2148 m to 2061m (7048 ft – 6763 ft; Fig. 4) exhibits gamma values of 100, porosities of 26 to 30%, and permeability that range from 50 to 125mD (Table 1; Fig. 10). Conversely, the Upper Stratigraphic Interval at 1829m to 1783 m (6000 ft – 5851 ft; Fig. 4), displays gamma values of 50 to 200, porosities of 8 to 25%, and permeability of less than 0.1 to 30 mD (Table 1; Fig. 10).

Overall, the porosity and permeability in the Lower Stratigraphic Interval are higher than those of the Upper Stratigraphic Interval. Furthermore, positive covariation trends of increasing porosity associated with increasing permeability are observed across the Lower to Upper Stratigraphic Interval depth horizons (Fig. 10). In addition, these patterns of porosity and permeability are also positively correlated with the gamma ray log (Fig. 10).

4.3 Paragenetic Sequence

Sidewall cores and thin section microscopic analyses of these lithologies have been synthesized into a comprehensive paragenetic sequence for the Mt. Simon Sandstone (Fig. 5). The paragenetic sequence is a relative spatial and temporal framework that integrates all of the observed depositional and diagenetic events observed within the Mt. Simon Sandstone (e.g. Fouke et al. 1996; Fouke et al. 2005). The ultrahigh-resolution (125 – 250 nm) petrographic analyses in this study is the first ever application of the Axiovert 200M Fluorescent Microscope with Apotome to sedimentary rocks. This has permitted a detailed evaluation of the relationships between sub-micron iron oxide cements, sutured quartz grains and quartz overgrowth cements, previously unattainable with standard microscopy. Results indicate that both the Lower and Upper Stratigraphic Intervals (Fig. 4) have experienced a similar suite of at least 7 paragenetic events (Fig. 5). Following deposition of the Mt. Simon Sandstone (Event 1), an early event of quartz grain contact suturing took place (Event 2; Fig. 11). This was followed by the precipitation of small spherical 1 to 5 μm diameter iron oxide cement (Event 3; Fig. 11). Although some of these iron oxide cements occur at sutured grain boundaries (Event 3; Fig. 11), they are interpreted to have precipitated after suturing within small pore spaces along the sutures (e.g. see blue-stained epoxy filling pore spaces along sutured grain boundaries in Fig. 11). These Event 3 (Fig. 5) iron oxide cements also precipitated on the outer surface of the quartz grains comprising the quartz arenite lithology (Event 3; Fig. 11).

This was followed by the precipitation of Event 4 clay cements (Fig. 5) on the outer surfaces of the Event 3 iron oxide cements (Event 4; Fig. 12). Two distinct syntaxial, euhedral quartz overgrowths then precipitated, both of which have a maximum thickness of approximately 50 μm (Events 5 and 6; Figs. 13, 14A- D). These two generations of quartz overgrowth cements exhibit distinct CL emissions, with Event 5 being non-CL (black) and Event 6 having dull-light blue CL (Fig. 14A-D). However, Events 5 and 6 were never observed growing one atop the other within pore space (Figs. 5 and 14). Therefore, their relative timing of precipitation with respect to each other remains uncertain (Fig. 5). The paragenetic sequence was then concluded with a final episode dark red iron oxide cement precipitation (Event 7) that coats the Event 5 and 6 euhedral quartz overgrowth cements (Fig. 15A- F).

4.4 Formation Water: Sr-Isotope Geochemistry

Sr- isotopic analyses of the Mt. Simon Sandstone formation water collected in the present study are presented in Table 1 and Figure 4. The $^{87}Sr/^{86}Sr$ analyses range from 0.71122 to 0.71158. These values are significantly more radiogenic than previous analyses of formation water from Pennsylvanian through Ordovician strata within the Illinois Basin (0.70789-0.71084; Stueber et al. 1987). In addition, the $^{87}Sr/^{86}Sr$ ratios of dissolved Sr in the Mt. Simon Sandstone formation water are 0.00222 to 0.00318 greater than the values that have been reconstructed for Cambrian seawater (Veizer et al. 1999; Fig. 16). These differences are significant, as $^{87}Sr/^{86}Sr$ ratios vary by a maximum of 0.00295 in the Pennsylvanian through Ordovician strata (Stueber et al. 1987; Fig. 16).

CHAPTER 5
DISCUSSION

5.1 Depositional History of the Mt. Simon Sandstone

The Lower Stratigraphic Interval of the Mt. Simon Sandstone is composed of moderately-well sorted, fine to medium grained quartz arenites with abundant iron oxide cements and relatively little quartz cement overgrowths (Figs. 4, 6, 7). Some of the sidewall cores extracted from the Lower Stratigraphic Interval exhibited cross-bedding on the scale of millimeters. This is further supported by the petrophysical data, which exhibited gamma values of 100, porosities of 26 to 30%, and permeability that range from 50 to 125mD (Table 1; Fig. 10). This type of moderately to well-sorted quartz arenite rock texture is consistent with first erosional cycle of sandstone deposition in hydrologically energetic environments, such as alluvial fans or nearshore marine zones, as well as mature sandstones derived from multiple cycles of fluvial erosion and extensive lateral transports (polycyclic; Boggs 2001).

However, the Mt. Simon Sandstone directly overlies a Precambrian crystalline basement that had mountains with up to 610 m (2000 ft) to topographic relief (Leetaru and McBride 2009). The Illinois Basin was near the equator during the Cambrian and in many areas the shallow Iapetus Ocean would have surrounded many of these mountains to form islands (McKerrow et al. 1992; Kolata 2010), which are environment conditions that likely precluded extensive lateral quartz sand transport. Therefore, the depositional environment of the Mt. Simon Sandstone in the Lower Stratigraphic Interval is interpreted as representing deposition in a first erosional cycle, high hydrologic energy environment dominated by terrestrial alluvial fans that formed prograding deltas into surrounding shallow marine shelf environments (Boggs 2001). In specific, the cross-bedded well-sorted clean quartz sands comprising the Lower Stratigraphic Interval are most consistent with deposition in the distal portion of a alluvial fan delta complex (Fig. 17), where a subaqueous delta plain experiences high-energy wave action (Boggs 2001). A modern analog for this type of deposition is the Kurobegawa Fan in Toyama Bay, which is prograding into central Japan Sea (Boggs 2001). Interpretations of alluvial fan to braided river depositional environments have been proposed for the “lower section” of the Mt. Simon Sandstone (Leetaru et al. 2009; Leetaru and McBride 2009; Bowen et al. 2011). However, these studies were

completed with coarse-scale sampling on a regional scale. Therefore, interpretations from the present study represent higher spatial-resolution refinements of the previous reconstruction for the Mt. Simon Sandstone.

The Upper Stratigraphic Interval is a moderately well-sorted quartz arenite with no cross-bedding that is interbedded with fine shale layers (Figs. 4, 8, 9). The increase in shale content and abundance of quartz overgrowth cements, with respect to the Lower Stratigraphic Interval, has significantly reduced the porosity (8-25%) and permeability (0.1-30mD; Table 1; Figs. 8, 9, 10). As was the case for lithologies comprising the Lower Stratigraphic Interval, the horizons comprised of moderately well-sorted quartz arenites are consistent with deposition within terrestrial alluvial fan deltas that prograded into surrounding shallow marine environments (Boggs 2001). However, the occasional interbedding of fine shale layers suggest that deposition took place in a more proximal position on the alluvial fan delta, possibly within abandoned distributary channels (Boggs 2001). These results are consistent with, and further refine, previous more generalized studies of the upper Mt. Simon Sandstone, which have interpreted it to have been deposited in terrestrial to shallow-water marginal marine environments (Driese et al. 1981; Leetaru et al. 2009; Bowen et al. 2011).

5.2 Paragenesis of the Mt. Simon Sandstone

The Lower and Upper Stratigraphic Intervals of the Mt. Simon Sandstone exhibit nearly identical paragenetic sequences, with the exception that the Upper Stratigraphic Interval has a significantly greater abundance and presence of quartz overgrowth cements (Figs. 4, 5, 6, 8). The paragenetic sequence is directly related to, and ultimately strongly influenced by, the temperature and pressure burial history, which in the present circumstance began with surface deposition at the beginning of the Cambrian (~542 Ma; Rowan et al. 2002; Makowitz et al. 2006; Fig. 18). This was immediately followed by a period of early rapid subsidence and burial to a depth of approximately 0.4 km by the middle Cambrian (Rowan et al. 2002; Makowitz et al. 2006; Fig. 18). Specifically, the high overburden burial pressure established in this period of early rapid subsidence is most likely the environment in which the sutured quartz grain contacts were formed (Worden and Morad 2000; Event 1; Fig. 5). Previous work has shown that, instead of being controlled solely by depth-dependent lithostatic pressure, sutured quartz grain contacts are controlled by a combination of pressure (effective stress), temperature and clay content

(Thompson 1959; Ramm and Bjorlykke 1994; Worden and Morad 2000). These affects can be lowered by increased hydrostatic overpressures (Worden and Morad 2000). Thus, the precise depth represented by suturing is difficult to establish. For example, Taylor (1950) observed that sutured grain contacts first develop between burial depths of 2.08 km (6832 ft) in the Lower First Wall Creek Formation (fine-grained feldspathic sandstone) of Wyoming, while Weibel et al. (2010) observed sutured quartz grain contacts to form only at 3 km (9843 ft) in the Vaale Formation, Bor member (glauconitic quartz arenite to subarkose) in Siri Canyon in the Danish North Sea. Further, Thompson (1959) saw no evidence of sutured grains at depths greater than 5.18 km (17000 ft) within the Silurian Green Pond Conglomerate of northern New Jersey. The Mt. Simon Sandstone was never overpressured during subsidence due to the relatively slow overall rate of burial, low volume of shale deposition, and the laterally continuous basal Mt. Simon Sandstone aquifer (Bethke 1986). These sutured grain contacts may have also provided a source of dissolved silica for the precipitation of the quartz overgrowth cements (Events 5 and 6; Fig. 5). Similar local sourcing of quartz cement chemistries have been previously proposed for other basins (McBride 1989; Worden and Morad 2000; Trewin and Fallick 2009).

Subsidence of the Mt. Simon Sandstone continued slowly for the remainder of the Paleozoic (Rowan et al. 2002; Makowitz et al. 2006; Fig. 18), and while the Mt. Simon Sandstone was at relatively shallow burial depths, oxygenated formation waters could have caused the precipitation of the initial iron oxide cements around the grains (Event 3; Fig. 5). The base of the Mt. Simon Sandstone eventually reached a burial depth of approximately 1.8 km by the middle Permian (Rowan et al. 2002; Makowitz et al. 2006; Fig. 18). This was followed by another period of rapid subsidence that continued until the base of the Mt. Simon Sandstone reached depths of approximately 2.4 km and temperatures of more than 100˚C at the end of the Permian (Rowan et al. 2002; Makowitz et al. 2006; Fig. 18). Cessation of midcontinent rifting was then triggered by the ongoing Alleghenian-Ouachita orogeny and associated uplift of the Pascola Arch (McBride et al. 2003; Kolata and Nelson 2010). This also initiated gravity-driven paleofluid flow within the Illinois Basin (Bethke and Marshak 1990; Kolata and Nelson 1991; McBride et al. 2003), which has been dated with illite/smectite at 260 ± 35 Ma in middle Paleozoic strata of the Illinois Basin(Duffin et al. 1989). Soon afterward, quartz overgrowth cements precipitated in the Mt. Simon Sandstone (Events 5 and 6; Fig. 5). This can be inferred from fluid inclusion analyses of similar quartz overgrowth cements within the Mt. Simon

Sandstone yielded homogenization temperatures of 100-115°C at a depth of approximately 1664 m (5458 ft) from a burial brine with a salinity of greater than 20 wt% NaCl (Fishman 1997). The burial depths for the fluid inclusion data by Fishman (1997) are consistent with Upper Stratigraphic Interval of the study, which contains significantly more quartz overgrowth cements than the Lower Stratigraphic Interval. Following the second rapid subsidence, the Mt. Simon Sandstone uplifted slowly during the Mesozoic (Rowan et al. 2002; Makowitz et al. 2006; Fig. 18). This uplift could have driven oxygenated, recharging meteoric water into the Mt. Simon Sandstone, resulting in the precipitation of the second iron oxide cements coating the quartz overgrowths in the Lower and Upper Stratigraphic Intervals (Event 7; Fig. 5). The return to slow subsidence began in the Paleocene (~65 Ma) and continuing through the Cenozoic into the modern reaching a depth of 1.9 km (Rowan et al. 2002; Makowitz et al. 2006; Fig. 18).

Several studies have been conducted on the Mt. Simon Sandstone formation waters (e.g. Visocky et al. 1985; Siegel 1989). However, the wells from which these waters were sampled penetrated extremely shallow sections of the Mt. Simon Sandstone in the northern portions of the Illinois Basin. Furthermore, they do not provide a complete suite of elemental and isotopic water analyses. Therefore, interpretation of the origin and chemistry of the burial brines that precipitated the quartz cement overgrowths observed in the Mt. Simon Sandstone in the present study (Events 5 and 6; Fig. 5) has been completed using analogous formation water collected from Silurian and Devonian strata in the Illinois Basin (Stueber and Walter 1991). This approach was necessary because the geochemistry of recently collected Mt. Simon Sandstone formation water collected from the Illinois Basin – Decatur Project is currently being completed by the ISGS and the data were not yet available.

Formation water from Silurian to Devonian strata in the Illinois Basin has a chloride (Cl)/bromide (Br) ratio that plots near a modeled seawater evaporation trajectory (Carpenter 1978) that stopped short of halite precipitation (Stueber and Walter 1991; Fig. 19). The Cl/Br ratio during seawater evaporation remains linear because both Cl and Br are inert in most biological and diagenetic processes until the brine reaches halite saturation (Stueber and Walter 1991). At the point of halite precipitation Br (k_D= 0.032) will preferentially remain within the brine as the Cl is incorporated into the halite (Carpenter 1978; McCaffrey et al. 1987). This suggests that the Mt. Simon Sandstone formation water originated at the surface from evaporated

seawater (Stueber and Walter 1991). In addition, cation/Br ratios within the Silurian to Devonian strata formation water suggest water and rock interactions further modified the evaporated seawater (Stueber and Walter 1991). For example, sodium (Na)/Br and potassium (K)/Br ratios are both depleted in the Silurian-Devonian formation water when compared to normal modern-day seawater, and fall below the seawater evaporation trajectory (Riley and Chester 1971; Carpenter 1978; Stueber and Walter 1991; Fig. 19). This loss of Na is generally explained by the albitization of feldspar (Carpenter 1978; Land and Prezbindowski 1981; Stueber and Walter 1991) and simultaneous loss of K by the precipitation of potassium feldspar cements (Egeberg and Aagaard 1989). The albitization of feldspar has the reaction of (Worden and Morad 2000):

$$2KAlSi_3O_8 + 2.5Al_2Si_2O_5(OH)_4 + Na^+ = NaAlSi_3O_8 + 2KAl_3Si_3O_{10}(OH)_2 + 2SiO_2 + 2.5H_2O + H^+$$

This reaction will release quartz and is an additional potential source for the quartz overgrowths cement within the Mt. Simon Sandstone and possibly produce the clays (Event 3; Fig. 5) (Worden and Morad 2000). Furthermore, the evaporation of seawater and the resulting increase in Na would tend to drive this reaction forward to further enhance quartz cementation.

The spread along the seawater evaporation trajectory in Silurian and Devonian formation water Cl/Br ratio suggests that this modified subsurface evaporated seawater also experienced mixing with recharging meteoric water (Stueber and Walter 1991; Fig. 19). The interpretation of evaporated seawater mixing with meteoric water and/or seawater has been debated by Land and Prezbindowski (1981), arguing that formation waters are depleted in deuterium, relative to SMOW, inconsistent with isotopic fractionation during seawater evaporation (Stueber and Walter 1991). Knauth and Beeunas (1986) have extended the seawater evaporation trajectory with data from Holser (1979), which shows negative δD and hooking $\delta^{18}O$ values created by extreme extents of seawater evaporation (Fig. 20). Stueber and Walter (1991) suggests that if the saline endmember was located on the seawater evaporation trajectory, such as that shown in the δD and $\delta^{18}O$ covariance plot (Fig. 20), the formation water must have been diluted by mixtures of 50% meteoric water. This addition of meteoric water into the Mt. Simon Sandstone could be the source of oxygen to precipitate the multiple iron oxide cements coating the grains and quartz overgrowths in the Lower and Upper Stratigraphic Intervals (Events 3, 7; Fig. 5).

5.3 Source of the Mt. Simon Sandstone Formation Water based on $^{87}Sr/^{86}Sr$

The Mt. Simon Sandstone formation water analyses in the present study yielded $^{87}Sr/^{86}Sr$ ratios that are 0.00222 to 0.00318 greater than Sr-isotope ratios in Cambrian sewater (Veizer et al. 1999; Fig. 16). This implies that dissolved Sr was derived from a source other than connate sweater within the Illinois Basin. Potential sources include: (1) overlying Paleozoic shales; (2) granites and rhyolites comprising the Precambrian igneous crystalline basement; and (3) shales and sands within the Mt. Simon Sandstone. Several previous studies have concluded that Silurian and Devonian formation water in the Illinois Basin derived dissolved radiogenic Sr from the New Albany shale group (Stueber et al. 1987; Bethke et al. 1991; Stueber and Walter 1991). However, it is uncertain whether this would apply to the Mt. Simon Sandstone, which has no obvious vertical hydrologic connectivity with the overlying Eau Claire shale (Leetaru et al. 2009; Bowen et al. 2011). It is also possible that dissolved radiogenic Sr was derived from water-rock interaction with granites and rhyolites comprising the Precambrian basement (Clark and Fritz 1997). This hypothesis is viable due to the extensive contact between the Mt. Simon Sandstone and the Precambrian basement, which lateral dispersion could mix solutes from the basement upward through the Mt. Simon Sandstone. Further, the Precambrian basement would not have to contribute much radiogenic Sr because the $^{87}Sr/^{86}Sr$ ratio is likely very high (Clark and Fritz 1997). The third hypothesis of deriving radiogenic Sr from shales and sands within the Mt. Simon Sandstone appears to be feasible, as well. Since the Mt. Simon Sandstone is primarily derived from Precambrian igneous basement, a significant concentration of radiogenic rubidium (^{87}Rb) is expected (Clark and Fritz 1997). ^{87}Rb is directly linked to potassium (K) geochemistry, for which it will substitute readily for K^+ in potassium feldspar, and decay into the daughter product, ^{87}Sr, thus increasing the $^{87}Sr/^{86}Sr$ ratios (Clark and Fritz 1997). Furthermore, the radiogenic Sr within the thin shale beds that occur in the Mt. Simon Sandstone appears to be highly accessible. Stueber et al. (1987) conducted leachate experiments on later Paleozoic shale formations within the Illinois Basin, which liberated high Sr ratios of 0.72793 to 0.75472. It is therefore reasonable to extrapolate these values to the shale within the Mt. Simon Sandstone.

CHAPTER 6
CONCLUSIONS

Results from the present study have significantly advanced our understanding of depositional environment and subsurface diagenetic evolution of the Cambrian Mt. Simon Sandstone in the Illinois Basin. Two stratigraphic horizons were samples and analyzed, which included: (1) a Lower Stratigraphic Interval at 2148 m to 2061m (7048 ft – 6763 ft); and (2) an Upper Stratigraphic Interval between 1829m to 1783 m (6000 ft – 5851 ft). The Lower Stratigraphic Interval is composed of a porous and permeable, moderate to well-sorted quartz arenite consistent with deposition at the distal margins of a terrestrial alluvial fan delta that prograded into surrounding shallow-shelf marine environments. The Upper Stratigraphic Interval consists of a similar moderately well-sorted quartz arenite, with the addition of interbedded fine-grained shale layers that suggest deposition at a more proximal position within abandoned distributary channels on the alluvial fan delta complex.

The Lower and Upper Stratigraphic Intervals have experienced similar paragenetic histories. The exception is that the Upper Stratigraphic Interval exhibits a significantly greater abundance of quartz overgrowth cements coating the host rock quartz grains. Plane-light (PL), polarized-light and cathodoluminescence-light (CL) microscopy has been used to document a multistage paragenetic sequence in both the Lower and Upper Stratigraphic Intervals. This is comprised of grain contact suturing during an early compaction event, followed by dark red iron oxide (hematite and goethite) and clay cement precipitation. Two subsequent events of syntaxial, euhedral quartz cement overgrowths were then followed by a final event of iron oxide cementation on the quartz cement overgrowths.

Two distinct quartz overgrowth cements have been observed that served to indurate the rock, occlude porosity and reduce permeability. These quartz cement overgrowths may have formed during late Paleozoic and early Mesozoic of the burial history of the Mt. Simon Sandstone, when temperatures reached more than 100°C (Rowan et al. 2002; Makowitz et al. 2006). This is consistent with fluid inclusion homogenization temperatures of 100 to 115˚C derived from quartz overgrowth cements in other locations in the Illinois Basin that are closely correlated with the Upper Stratigraphic Interval (Fishman 1997). The silica for the quartz overgrowth cements may have been sourced from sutured grain contacts and albitization of

feldspar in diagenetic brines (Worden and Morad 2000; Trewin and Fallick 2009). Furthermore, these overgrowths may have formed around Alleghenian-Ouachita orogeny, which changed burial depth and temperatures, as well as gravity-driven flow through the Illinois Basin (Bethke 1986; Bethke and Marshak 1990; Bethke et al. 1991).

$^{87}Sr/^{86}Sr$ analyses of the Mt. Simon Sandstone formation water in the present study yielded ratios of 0.7112 to 0.71158 ±0.00003. These values are significantly more radiogenic than previous analyses of formation water from Pennsylvanian through Ordovician strata within the Illinois Basin (Stueber et al. 1987). In addition, the $^{87}Sr/^{86}Sr$ of dissolved Sr in the Mt. Simon Sandstone formation water is 0.00222 to 0.00318 greater than the $^{87}Sr/^{86}Sr$ reconstructed for Cambrian seawater (Veizer et al. 1999; Fig. 16). While other source in the Illinois Basin were considered, it is possible that this dissolved radiogenic Sr was derived from sands and shales within the Mt. Simon Sandstone or the Precambrian basement.

CHAPTER 7

FIGURES

Figure 1: Location map showing the central position of Decatur within the Illinois Basin with an insert of the USA showing the location of the Illinois Basin, as well as the primary structural features surrounding the basin (modified from Buschbach and Kolata (1991); Kolata and Nelson (2010)). Cross-sections A-A' and B-B' are presented in Figure 2.

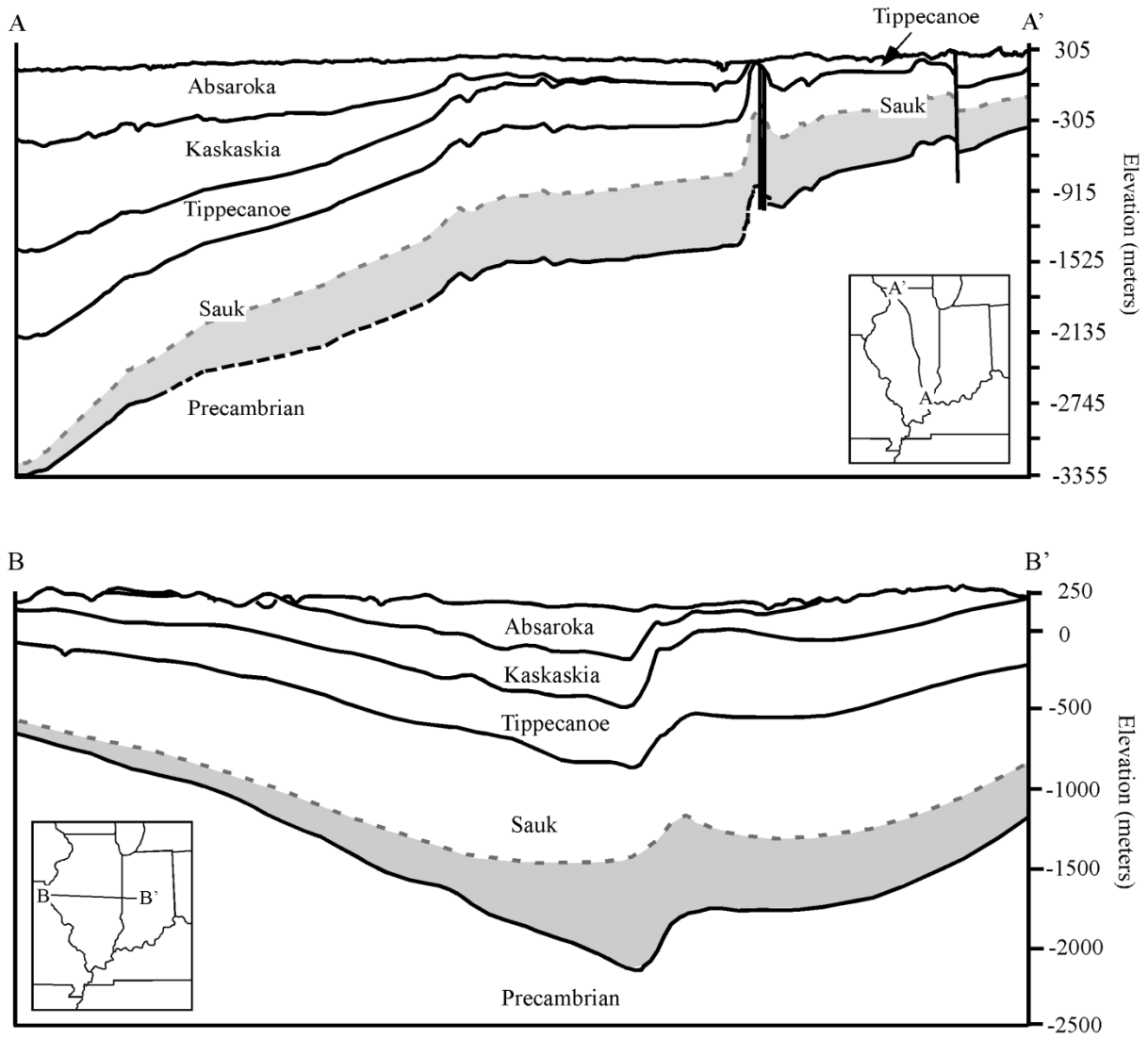

Figure 2: North-south (A-A') and east-west (B-B') cross-sections through the Illinois Basin showing the major depositional sequences and the Mt. Simon Sandstone (gray shaded strata). Modified from Buschbach and Kolata (1991), Kolata (1991), Treworgy et al. (1997) and Kolata and Nelson (2010).

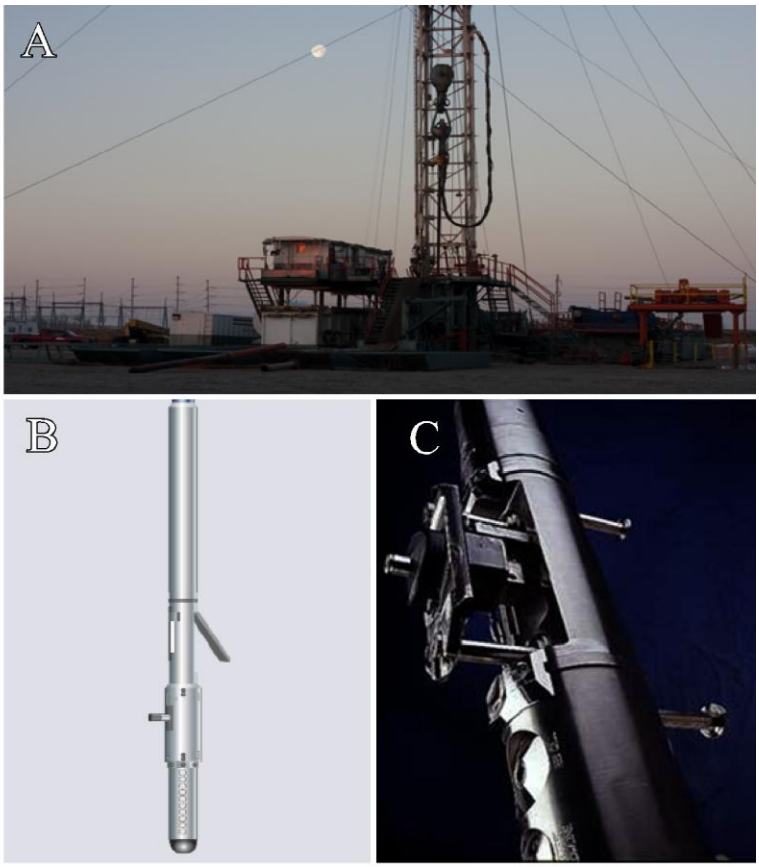

Figure 3: Sampling equipment. A: Schlumberger drilling rig used to penetrate to the Mt. Simon Sandstone at Decatur, Illinois for the Illinois Basin – Decatur Project CCS well (by permission from the ISGS). B: The Schlumberger mechanical sidewall coring tool (MSCT) used to collect rock samples (https://www.slb.com). C: The Schlumberger Modular Formation Dynamics Tester (MDT) with Quicksilver Probe used to collected formation water (https://www.slb.com).

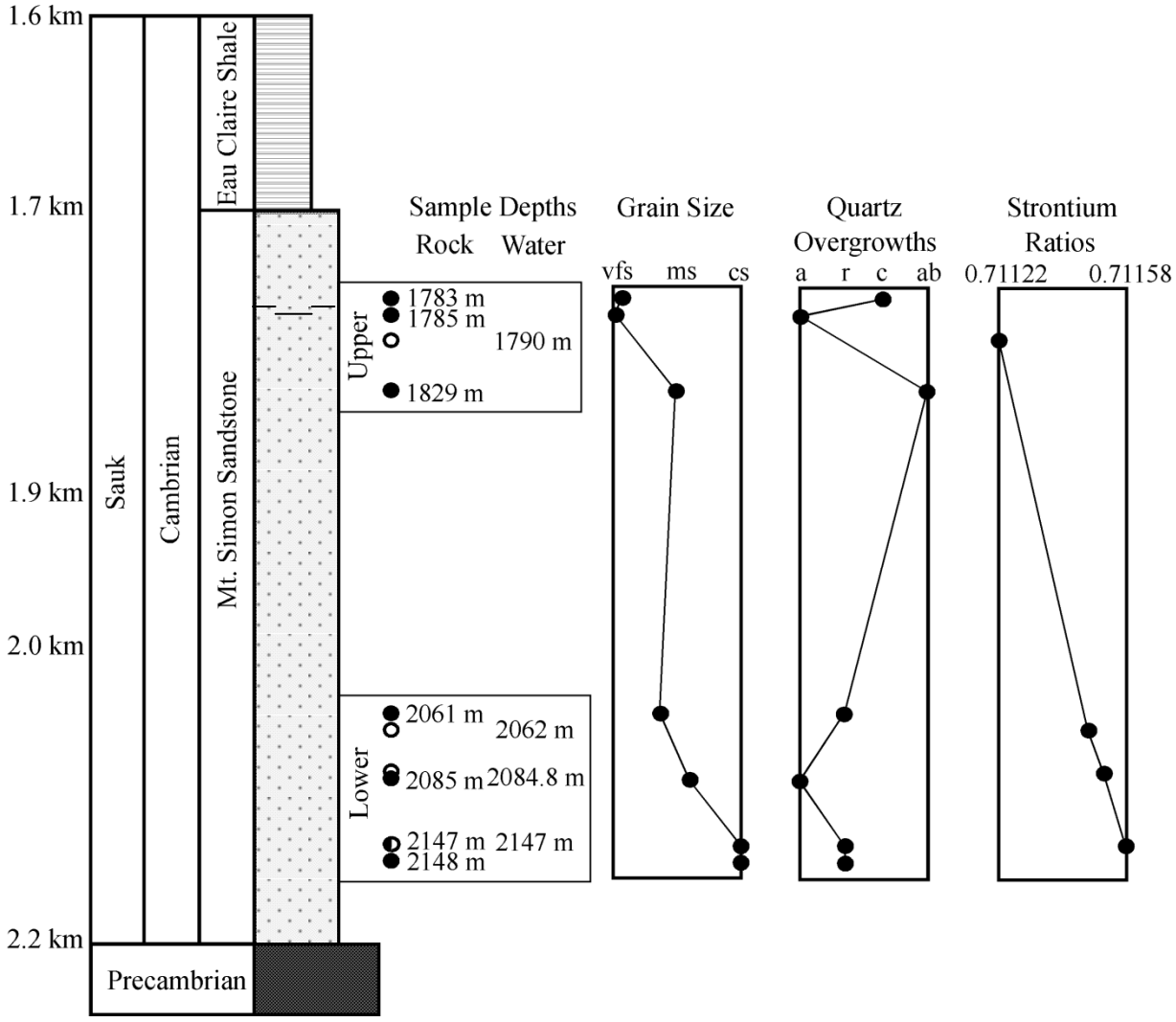

Figure 4: Stratigraphic sequence at the bottom of the Illinois Basin penetrated by the Illinois Basin – Decatur Project CCS well, including the Precambrian crystalline basement, the Cambrian Mt. Simon Sandstone and the overlying Cambrian Eau Claire Shale. Lower and Upper Stratigraphic Intervals are show with the elevation of the formation water samples (white circles) and sidewall cores (black circles) analyzed in the present study. Grain size for each depth studied is plotted on a scale of very fine sand (vfs), medium sand (ms), and coarse sand (cs). Quartz overgrowth abundances are plotted for each depth from this study on a scale of absent (a), rare (r), common (c), and abundant (ab). Corresponding $^{87}Sr/^{86}Sr$ ratios are also provided for the formation water samples.

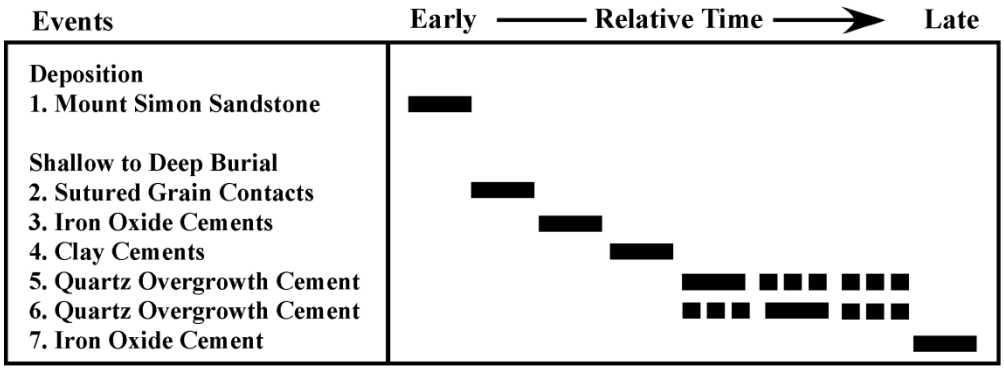

Figure 5: Paragenetic sequence from this study of the Mt. Simon Sandstone at Decatur, Illinois from the depths of 1.8-2.1 km.

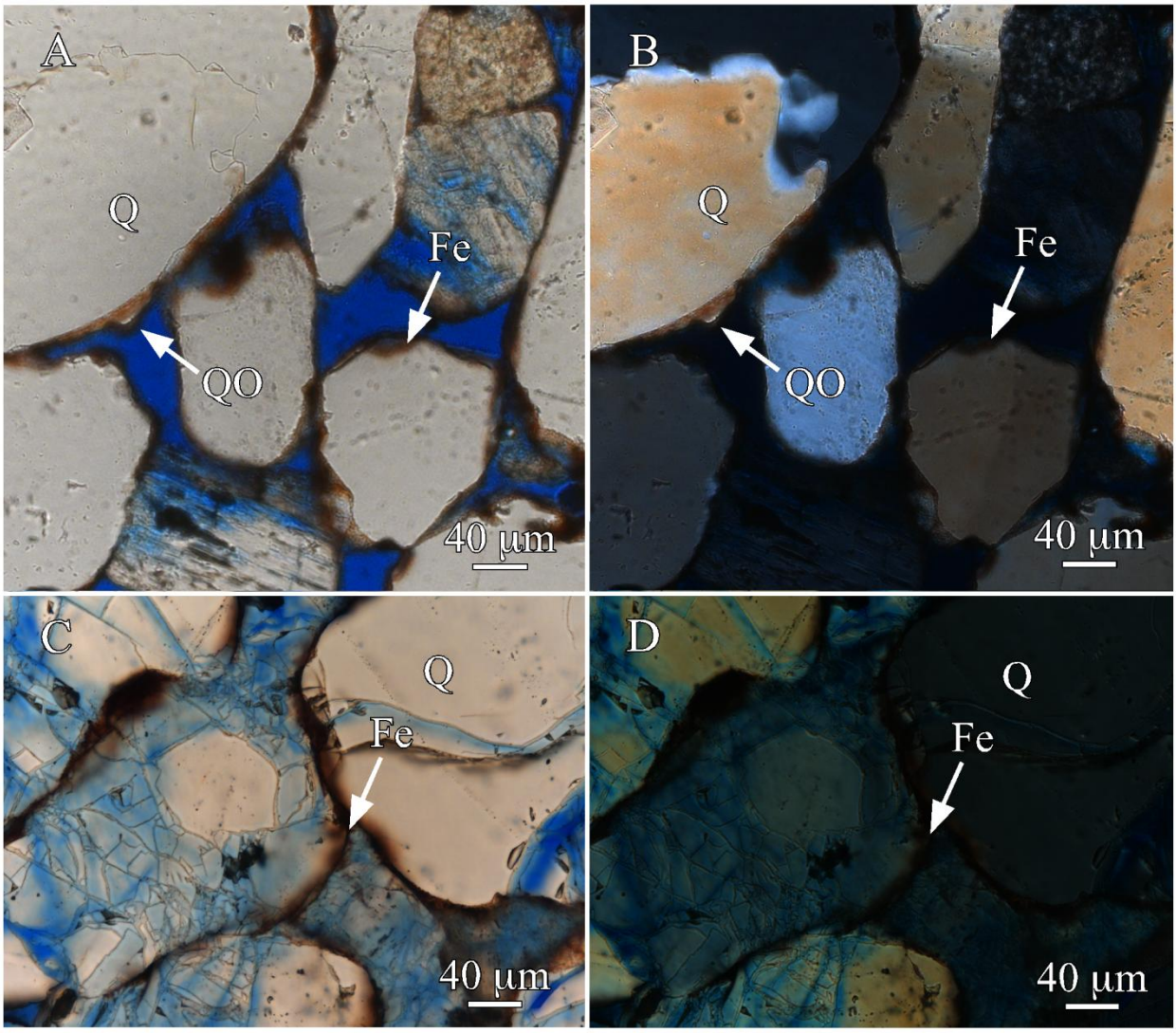

Figure 6: Paired PL and polarized-light photomicrographs illustrating the lithologic composition of the Mt. Simon Sandstone at the Lower Stratigraphic Interval. A and B are from the burial depth of 2148 m (7048 ft) and is a quartz arenite with small abundances of quartz overgrowths and each grain is coated in a dark red iron oxide rim. C and D are from the depth of 2147 m (7045 ft) composed of mainly quartz grains (quartz arenite) with iron oxide rims and rare quartz overgrowths. The grains have conchoidal fractures, most likely a consequence of sampling. Q: quartz grain; QO: quartz overgrowths; Fe: iron oxide (hematite or goethite).

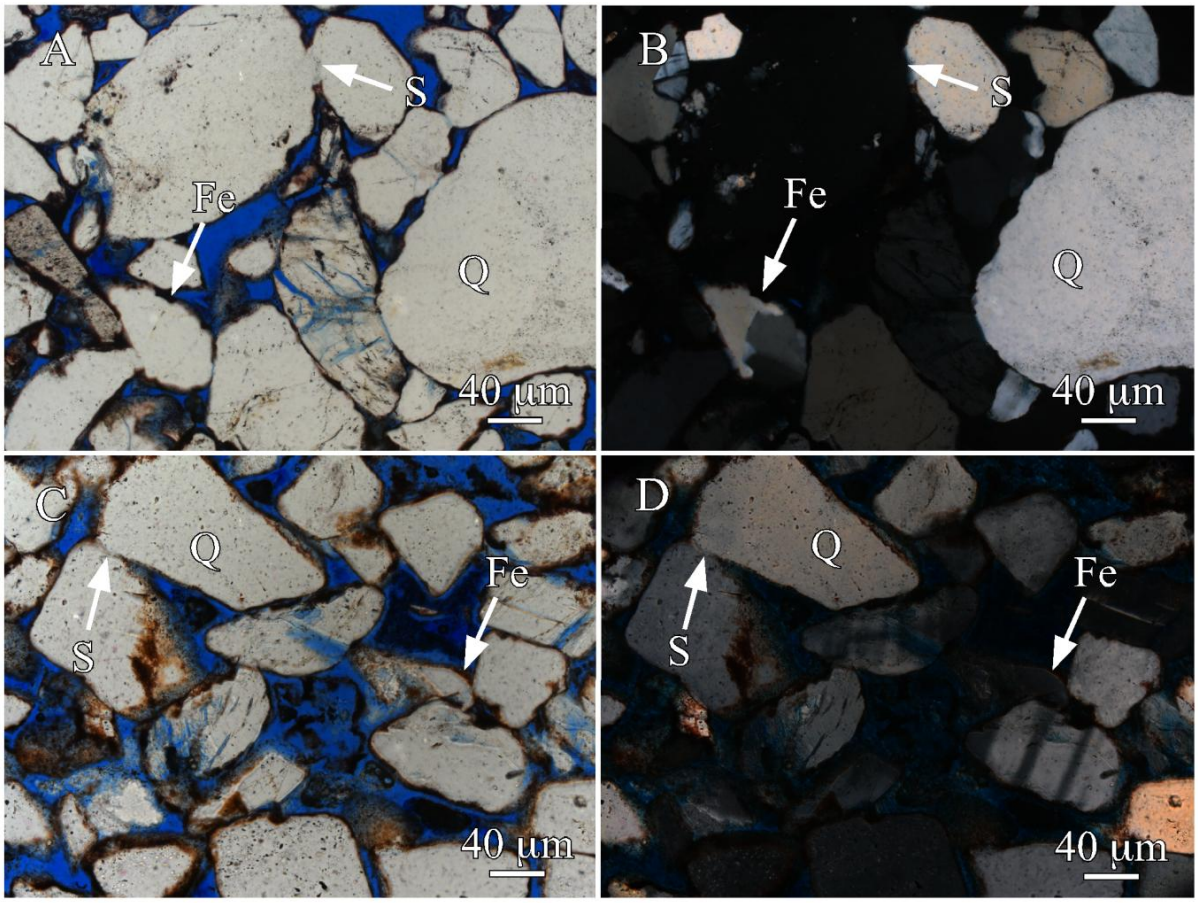

Figure 7: Paired PL and polarized-light photomicrographs illustrating the lithologic composition of the Mt. Simon Sandstone at the Lower Stratigraphic Interval. At a burial depth of 2085 m (6841 ft), A and B represent a quartz arenite with no quartz overgrowths, dark red iron oxide coated grains, and sutured contacts. C and D are from the depth of 2061 m (6763 ft) and are composed of a quartz arenite with sutured contacts and a rare abundance of quartz overgrowth cements. The grains are also coated with an iron oxide cement rim. Q: quartz grain; Fe: iron oxide (hematite or goethite); S: sutured contact.

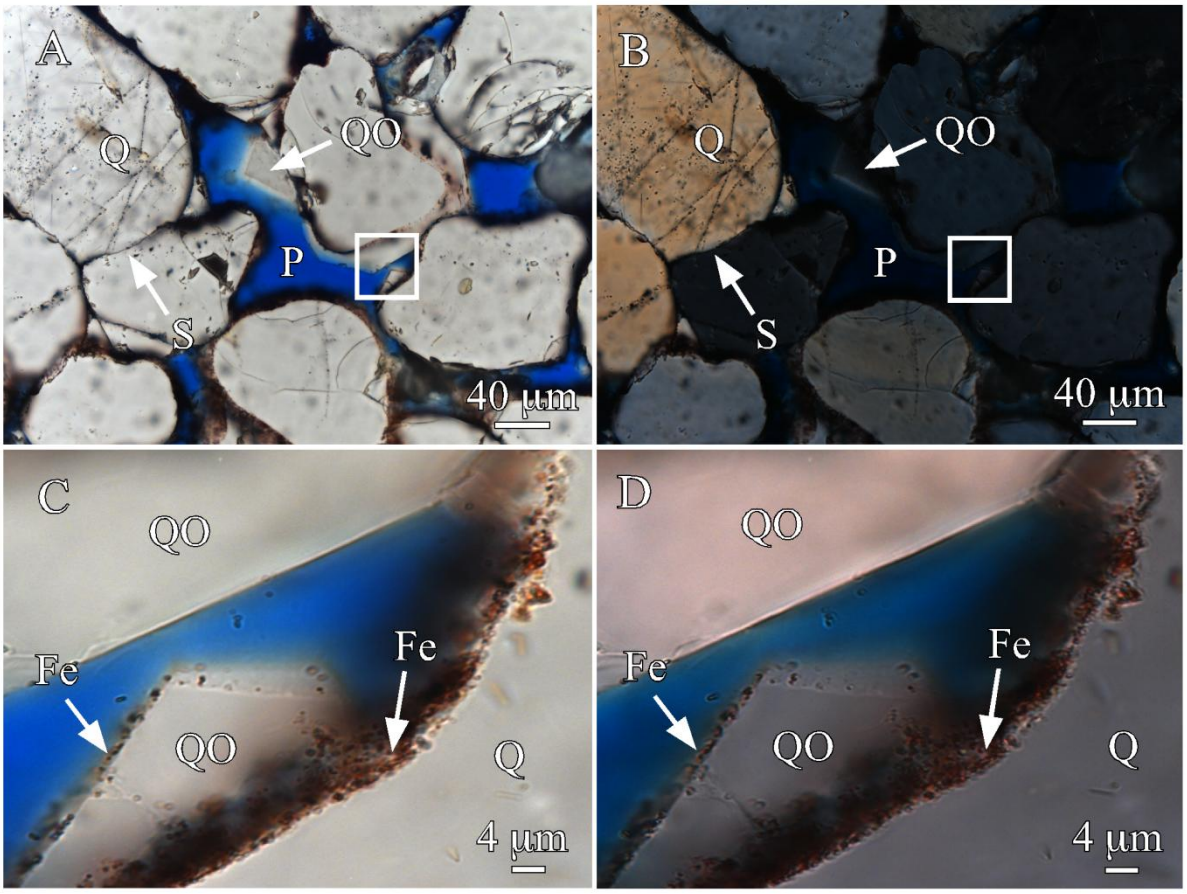

Figure 8: Paired PL and polarized-light photomicrographs illustrating the lithologic composition of the Mt. Simon Sandstone at the Upper Stratigraphic Interval. A and B (1829 m [6000ft]) represent a quartz arenite with abundant quartz overgrowths, dark red iron oxide coated grains, and sutured contacts. C and D are photomicrographs taken from the white box outline in A and B. C and D show the spatial relationship of the iron oxide cement with the surrounding quartz overgrowth cements in more detail. Q: quartz grain; QO: quartz overgrowths; Fe: iron oxide (hematite or goethite); S: sutured contact; P: porosity.

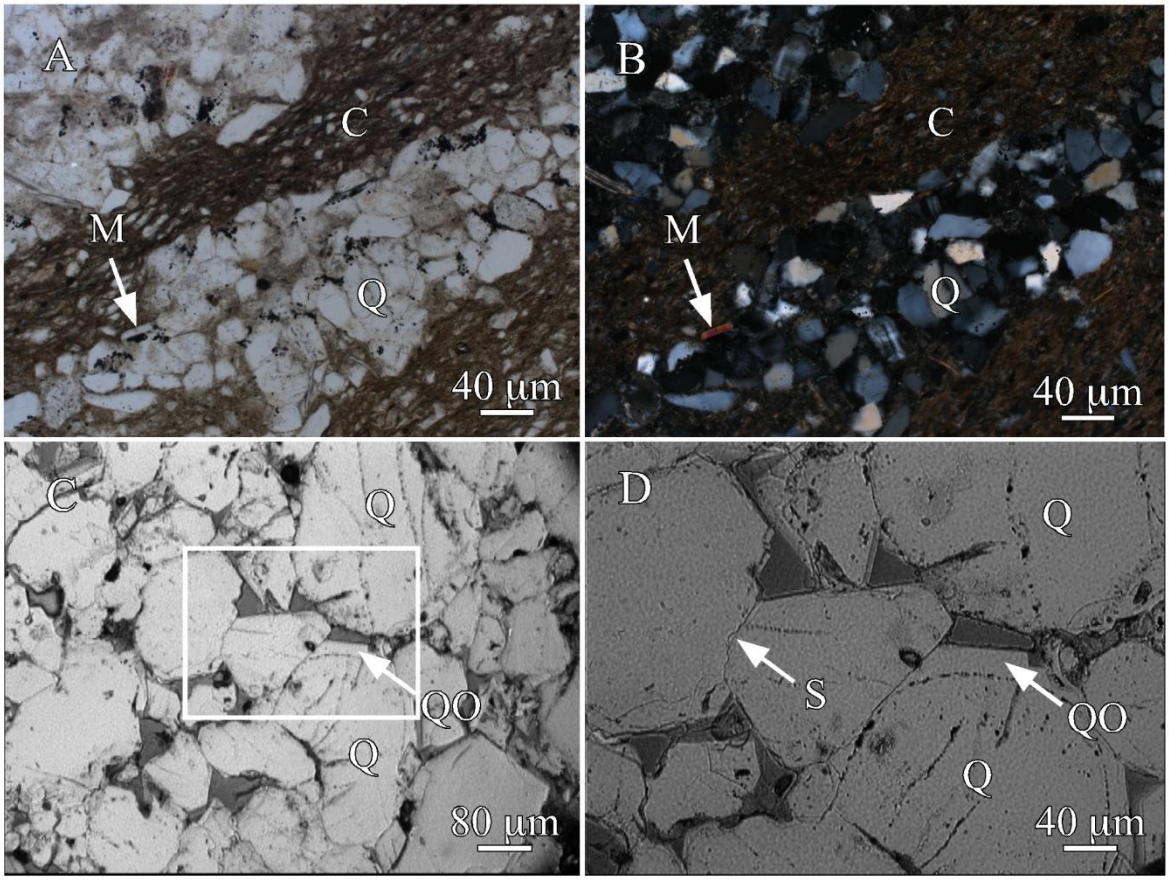

Figure 9: A and B are paired PL and polarized-light photomicrographs from a depth of 1785 m (5856 ft). The quartz grains are interbedded with mudrock (shale), which contains some mica. There is an absence of quartz overgrowths and no visible porosity and permeability. C is a PL photomicrographs at a burial depth of 1783 (5851 ft) and D is the photomicrograph from the area of the white box in C. C and D consist of a quartz arenite, with common quartz overgrowths and sutured grain contacts. Q: quartz grain; QO: quartz overgrowth; C: clay-silt particles; S: sutured contact; M: mica.

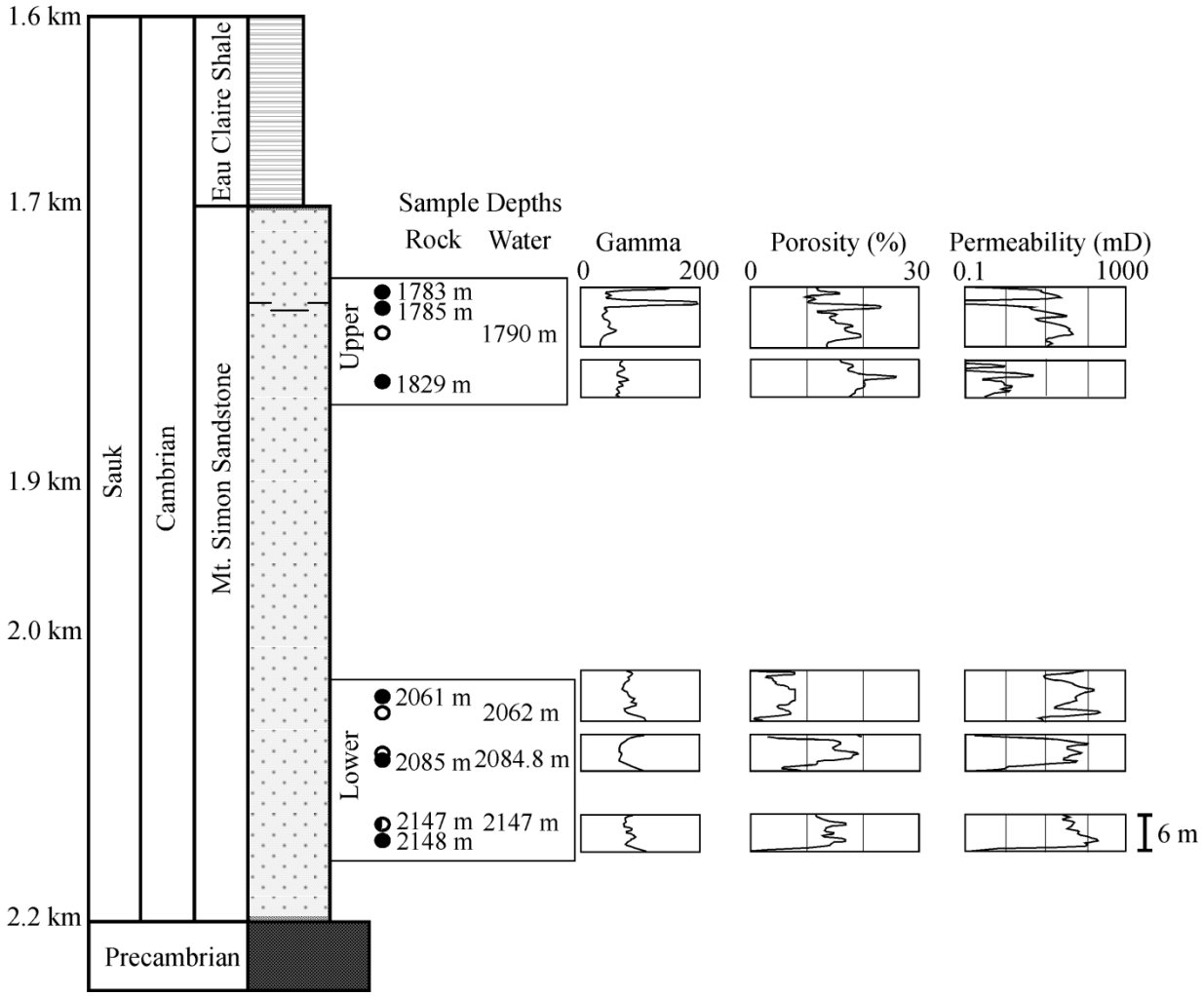

Figure 10: Stratigraphic sequence at the bottom of the Illinois Basin penetrated by the Illinois Basin – Decatur Project CCS well, including the Precambrian crystalline basement, the Cambrian Mt. Simon Sandstone and the overlying Cambrian Eau Claire Shale. Lower and Upper Stratigraphic Intervals are outlined with the elevation of the formation water samples (white circles) and sidewall cores (black circles) analyzed in the present study. Gamma radiation (gamma ray tool), porosity (neutron porosity tool) and permeability (nuclear magnetic resonance tool) collected by Schlumberger are shown with a vertical exaggeration of 10X (scale bar for the logs is shown in the lower right).

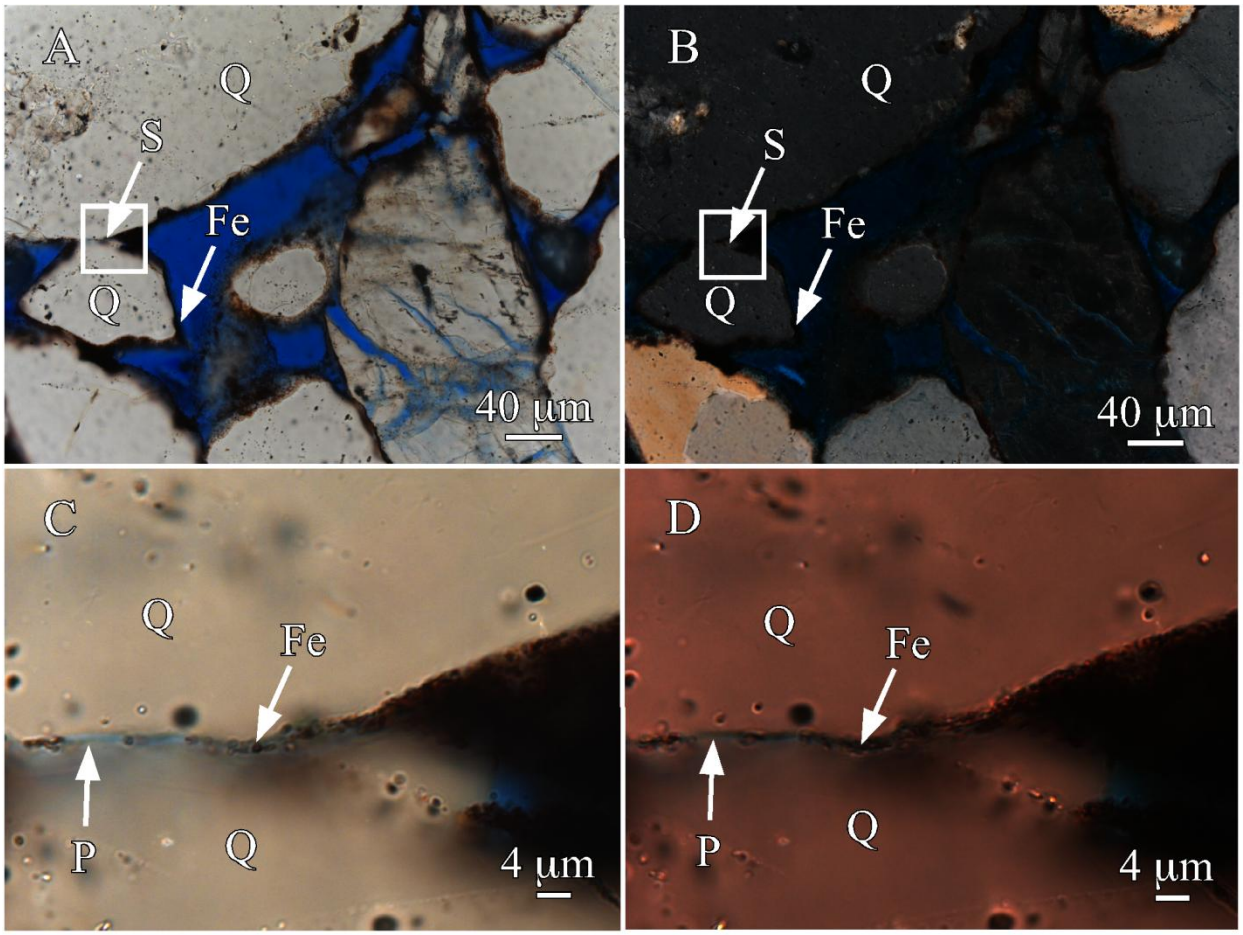

Figure 11: Paired PL and polarized-light photomicrographs illustrating Event 2 and 3 of the paragenetic sequence. A and B (2085 m [6841ft]) represent a quartz arenite that has undergone compaction, as seen from the sutured contacts. C and D are photomicrographs taken from the white box outline in A and B showing the sutured contact in more detail. While iron oxide is present within the suture, the ultrahigh-resolution microscopy shows blue pore space within the suture were the iron oxides are located, thus the iron oxides within the sutures do not pre-date the sutures themselves (Event 2). Event 3, the iron oxide cement coating, is seen surrounding the grains in A and B. Q: quartz grains; Fe: iron oxide (hematite or goethite); S: sutured contact; P: porosity.

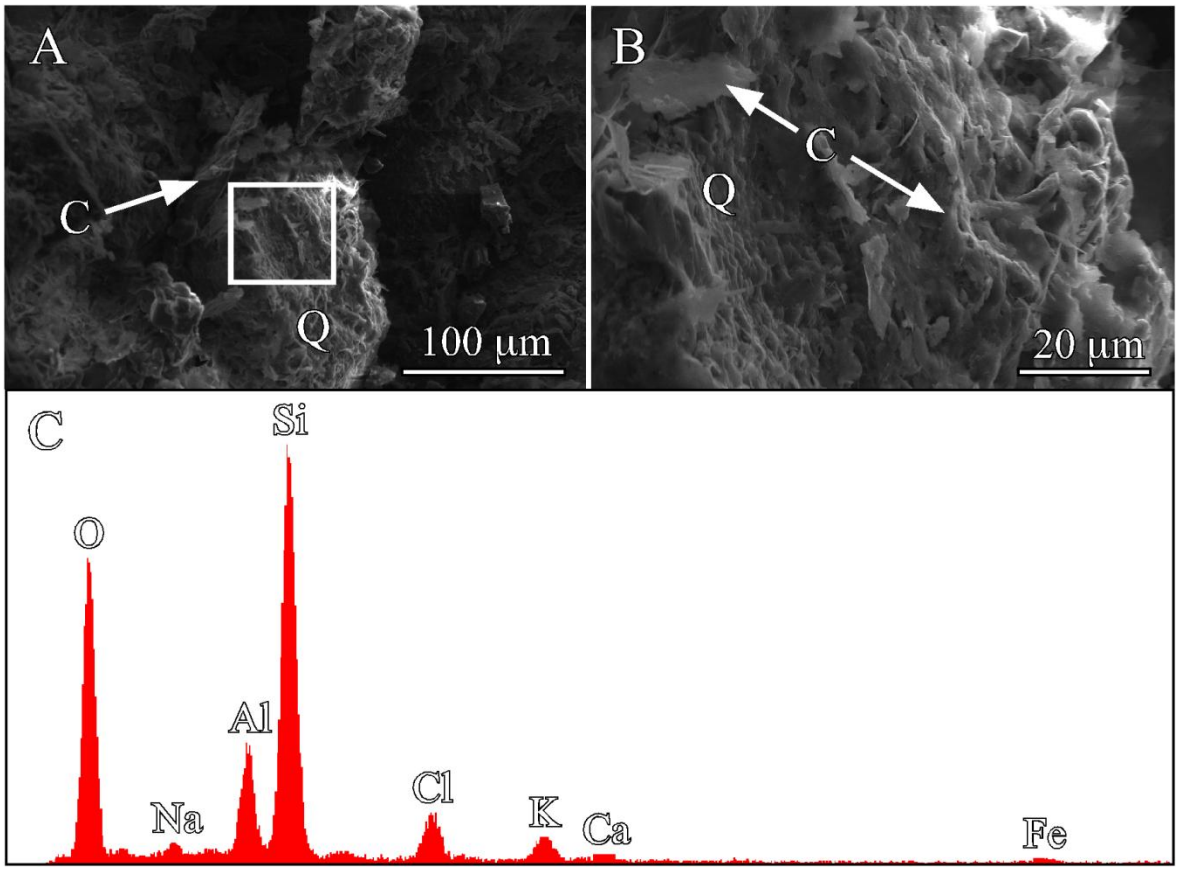

Figure 12: Environmental scanning electron microscope (ESEM) photomicrographs, A and B, of a rock sample from a depth of 1961 m (6433 ft), show Event 4 of the paragenetic sequence. B was taken from the area of the white box in A. A and B show the abundance of clay particles coating quartz grains and the presence of the clay particles, without iron oxide cement on top of them, indicate the clay post-dates the iron oxide precipitation (Event 3). C is a histogram produced from energy-dispersive spectroscopy (EDS) data illustrating the elements present within the photomicrographs A and B. Silica (Si) and oxygen (O) dominate the histogram because of the quartz grains present and the relative amounts of aluminum (Al), sodium (Na), chlorine (Cl), potassium (K), calcium (Ca) and iron (Fe) are a response from the clays present. Q: quartz grain; C: clay particles

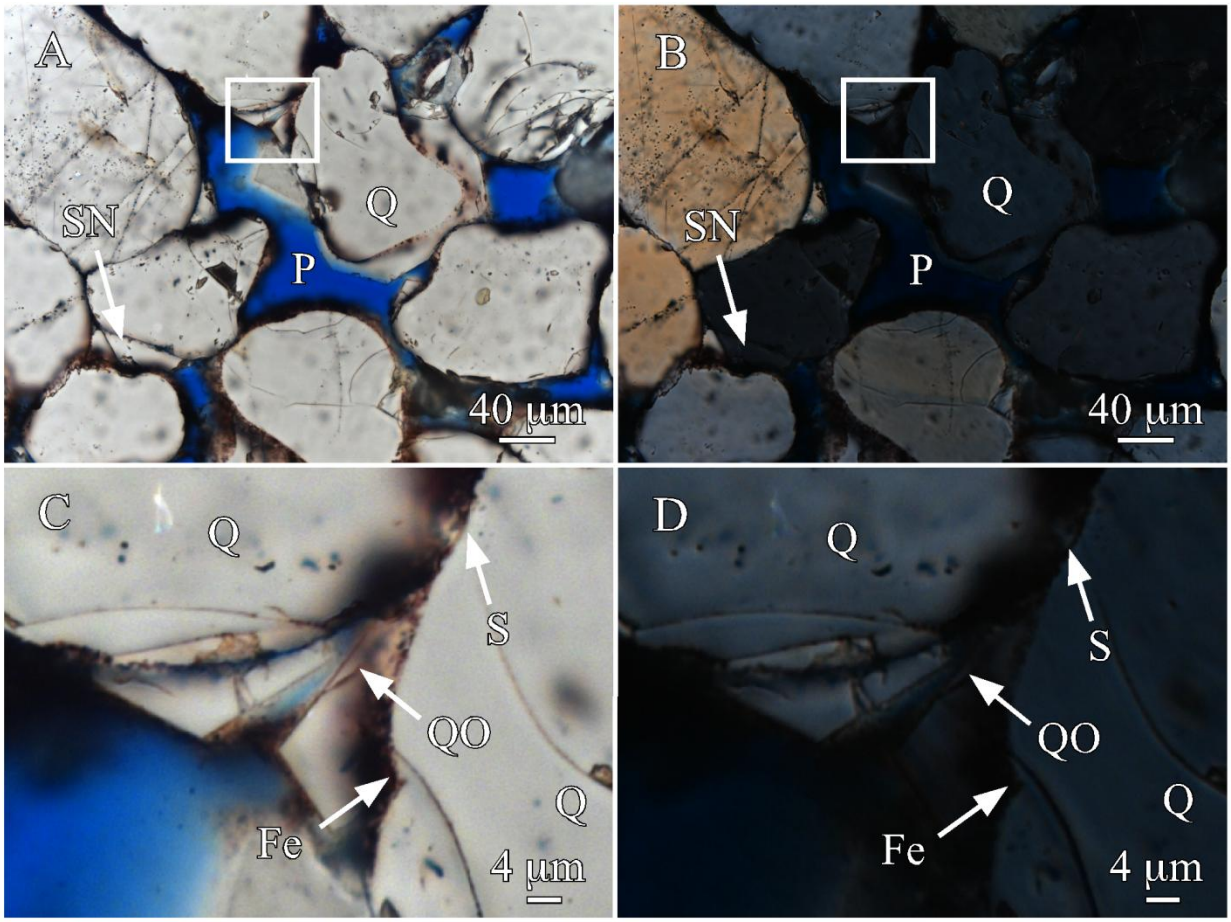

Figure 13: Paired PL and polarized-light photomicrographs illustrating Events 5 and 6 of the paragentic sequence. A and B from 1829 m (6000ft) show the syntaxial, euhedral quartz overgrowths (same polarization color as the grains; example marked by SN arrows) and have the location of photomicrographs C and D, outlined in the white box. C and D show the temporal relationship iron oxide cement, sutured contacts and quartz overgrowths. The sutured contact (S) is followed by iron oxide precipitation coating the grain (Event 2 and 3, see Fig. 11), followed by euhedral quartz overgrowth cements precipitating over the suture contact, thus post-dating the compaction event (Event 5 and 6). Q: quartz grain; QO: quartz overgrowths; Fe: iron oxide (hematite or goethite); S: sutured contact; P: porosity; SN: syntaxial quartz overgrowth.

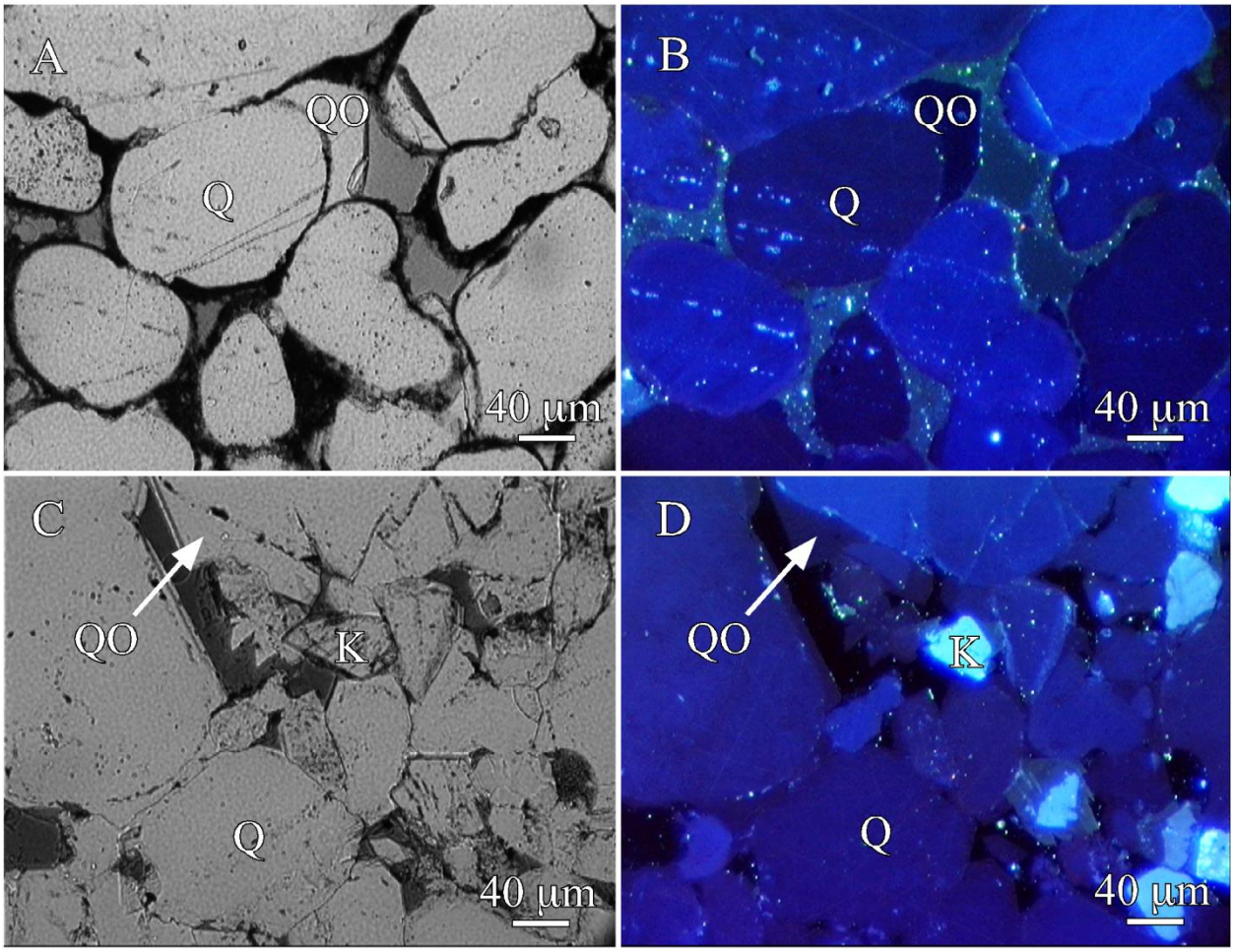

Figure 14: Paired plane-light and cathodoluminescene-light (CL) photomicrographs of the Mt. Simon Sandstone illustrating the Events 5 and 6 of the paragenetic sequence. Photomicrographs A and B taken at the burial depth of 1829 m (6000 ft) show the non-luminescence (black) quartz overgrowths. Photomicrographs C and D from the depth 1783 m (5851 ft) show a distinctly different the light-blue luminescence quartz overgrowth, noted at the end of the white arrow. Q: quartz grains; QO: quartz overgrowths, K: potassium feldspar.

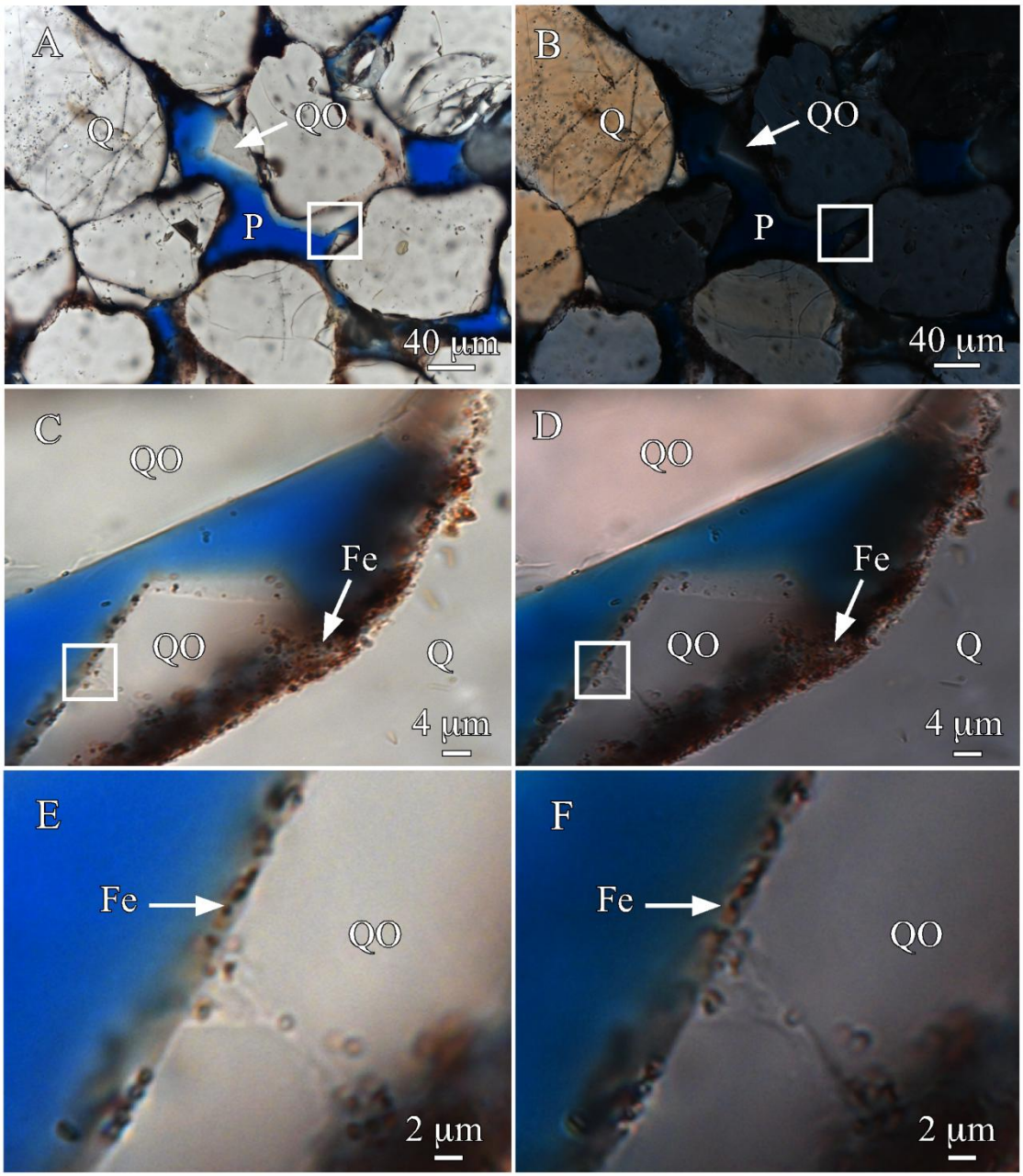

Figure 15: Paired PL and polarized-light photomicrographs illustrating Event 7 of the paragentic sequence. A and B from 1829 m (6000ft) have the location of photomicrographs C and D, outlined in the white box. E and F are photomicrographs from the white box within C and D. C and D show the temporal relationship between the first iron oxide cement coating the quartz grain (Event 3), which was then followed by the precipitation of quartz overgrowths (Event 5 and 6). E and F illustrate iron oxide cement (Event 7) coating the euhedral quartz overgrowth cements, indicating a second iron oxide precipitation event. Q: quartz grain; QO: quartz overgrowths; Fe: iron oxide (hematite or goethite); P: porosity.

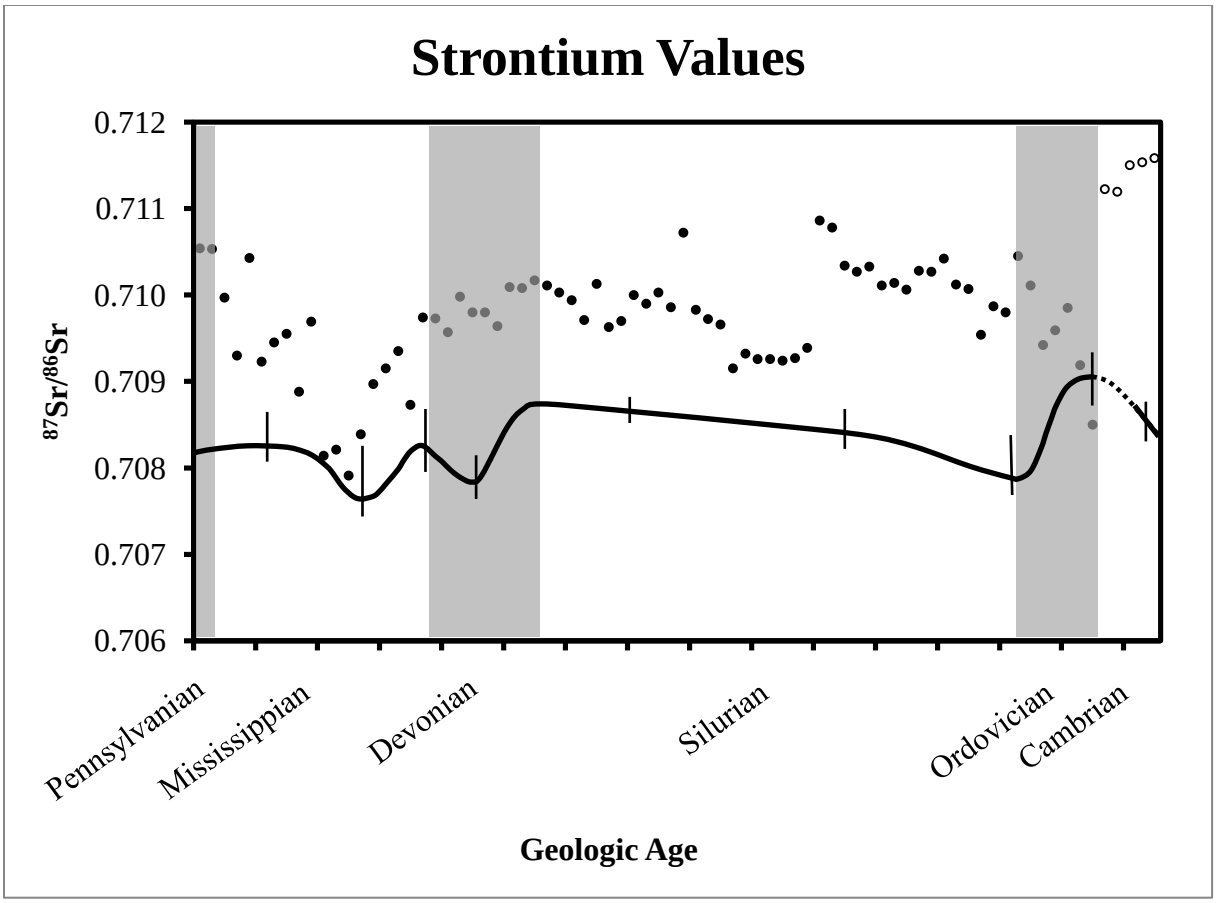

Figure 16: Modern day formation water $^{87}Sr/^{86}Sr$ compositions from lower Paleozoic strata (Pennsylvanian to Ordovician) (black dots) in the Illinois Basin from Stueber et al. (1987). Analyses in the present study of the Mt. Simon Sandstone formation watar (white circles) with error bars of ±0.00003. Secular variations in the strontium-isotope composition of Paleozoic seawaters (black line) from Veizer et al. (1999) with analytical error (vertical black lines). Gray boxes encompass the Sr-data for the geologic age of Pennsylvanian, Devonian and Ordovician (on the x-axis) Sr-data outside gray boxes correspond to the geologic age of Mississippian, Silurian, and Cambrian (on the x-axis). Both sets of data (Stueber et al. (1987) and this study (Cambrian)) have been standardized to the NBS 987 of 0.710240 from Veizer et al. (1999) for direct comparison to the secular seawater strontium-isotope curve.

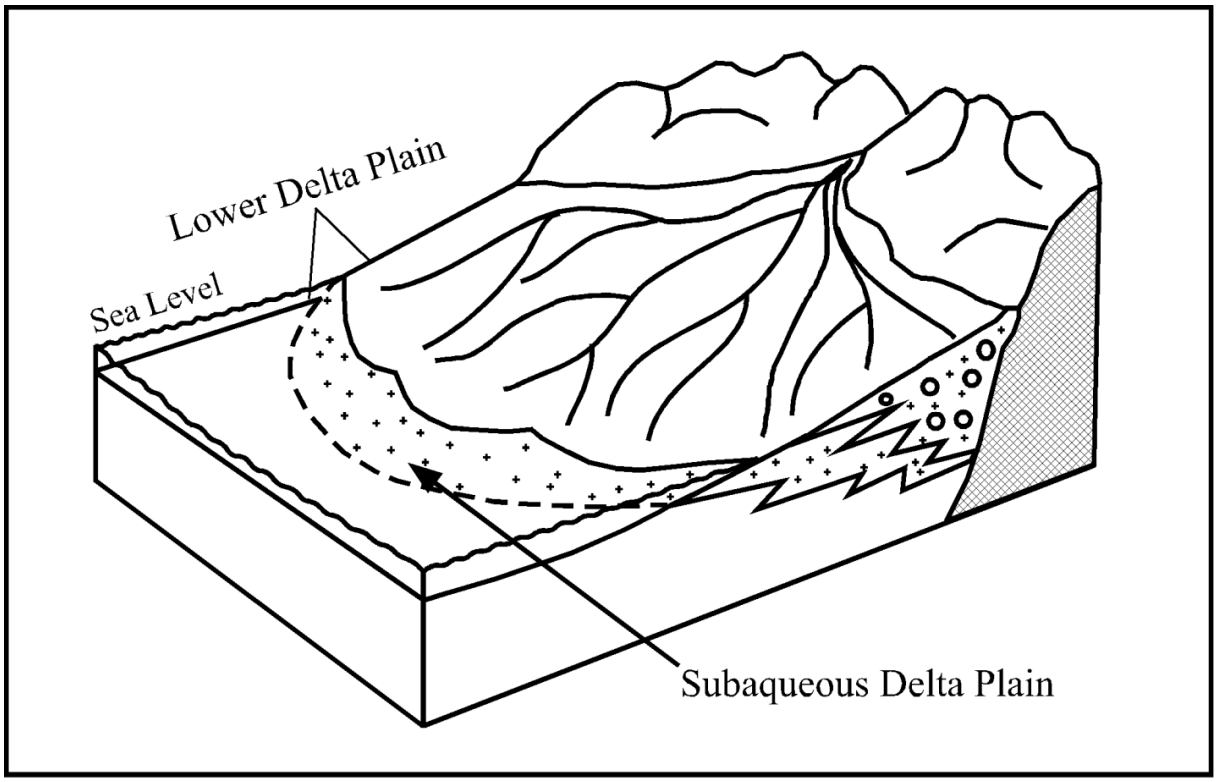

Figure 17: Illustration of a fan delta showing the relative locations of the subaqueous delta plain and the lower delta plain environments. The subaqueous delta plain is dominated by high-energy marine processes, such as wave action, and is always submerged. The lower delta plain is located between the low-tide mark and the high-tide limit and has deposits that range from sands to muds within distributary channels. Modified from Boggs (2001).

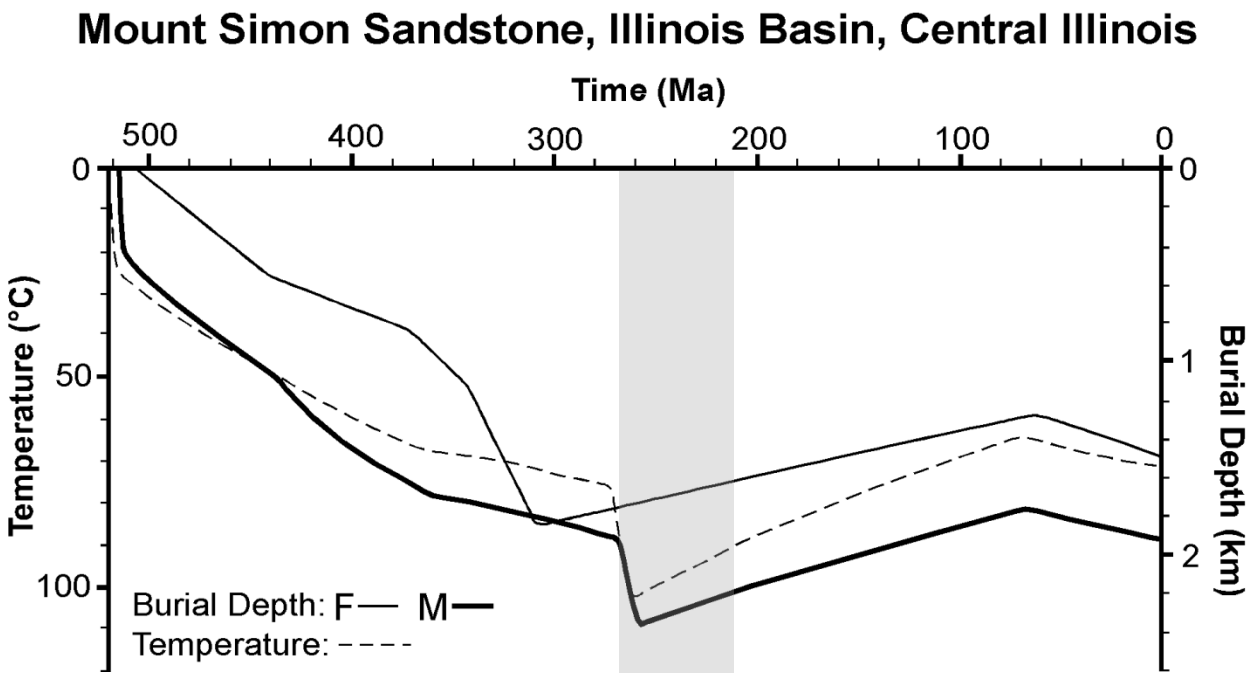

Figure 18: Burial history of the Mt. Simon Sandstone in central Illinois, modified from Fishman (1997) and Makowitz et al. (2006). F represents the burial depths from Fishman (1997) and M represents the burial depths from Makowitz et al. (2006). All temperature data is from Makowitz et al. (2006). Gray shaded area indicates timing of quartz overgrowth cement precipitation (late Paleozoic to early Mesozoic).

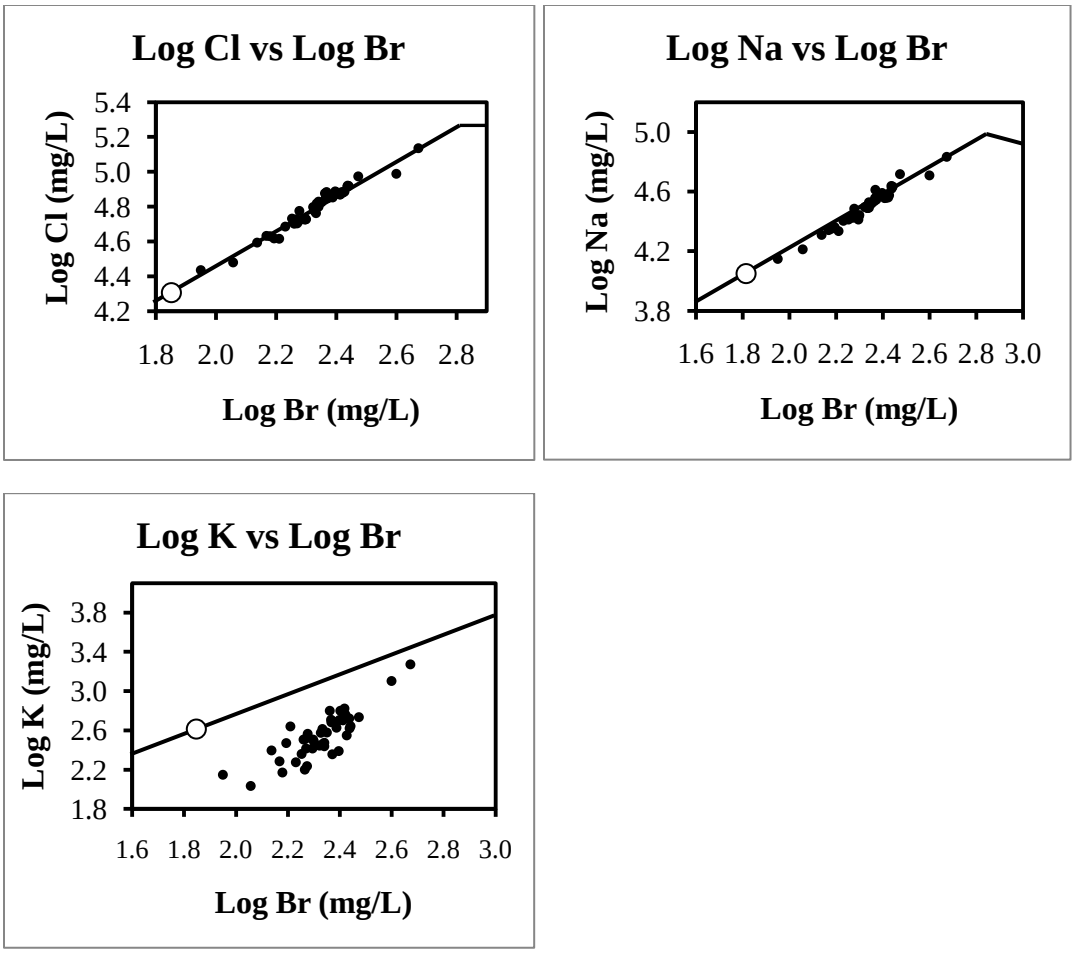

Figure 19: Covariation diagrams of Cl, Na, K, versus Br from Stueber and Walter (1991). The black line shown is the seawater evaporation trajectory established by Carpenter (1978) and white circle indicates the composition of seawater and evaporation is to the right of this circle following the line.

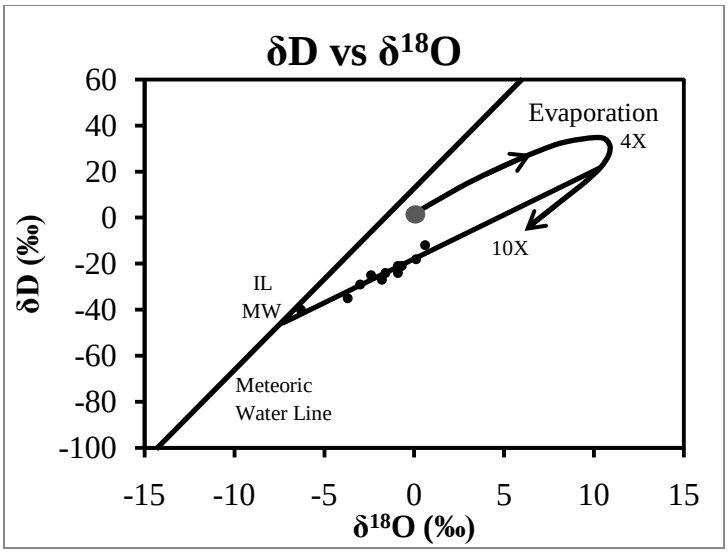

Figure 20: Covariation diagrams of δD versus $\delta^{18}O$ (per mil SMOW) from Stueber and Walter (1991). The present-day Illinois meteoric water (labeled IL MW) is from Clayton (1966). The evaporation trajectory from Kneath and Beenuas (1986) with data from Holser (1979) starts from SMOW (gray dot) and with continued evaporation towards 4X and 10X evaporation, the trajectory creates a hooked or curved trajectory back to negative δD values. A regression line is drawn through the data collected by Stueber and Walter (1991) and the IL MW, which intersects the evaporation curve between 4X and 10X evaporation, indicating Stueber and Walter (1991) samples evaporated to a point before halite precipitation (at 10X evaporation).

Depth (m)	Sample type	Porosity (%)	Permeability (mD)	$^{87}Sr/^{86}Sr$
1783	Rock	8.0	15	-
1785	Rock	20.5	<0.1	-
1790	Water	16.5	30	0.71122
1829	Rock	14.0	4	-
2061	Rock	30.0	53	-
2062	Water	30.0	51	0.71150
2084.8	Water	27.5	80	0.71153
2085	Rock	26.0	50	-
2147	Rock, Water	30.0	125	0.71158
2148	Rock	27.0	70	-

Table 1: Porosity and permeability data collected by Schlumberger wireline tools (neutron porosity tool and nuclear magnetic resonance tool). Formation water was collected with the Schlumberger Modular Formation Dynamics Tester with Quicksilver Probe and analyzed for Sr ratios using a Nu Plasma HR MC-ICP-MS at University of Illinois at Urbana-Champaign. The Sr ratios have been corrected to NBS 987 of 0.710240 from Veizer et al. (1999).

CHAPTER 8

REFERENCES

Bao, M. T., X. P. Kong, et al. (2009). "Laboratory study on activating indigenous microorganisms to enhance oil recovery in Shengli Oilfield." Journal of Petroleum Science and Engineering **66**(1-2): 42-46.

Bethke, C. M. (1985). "A numerical-model of compaction-driven groundwater-flow and heat-transfer and its application to the palohydrology of intracratonic sedimentary basins " Journal of Geophysical Research-Solid Earth and Planets **90**(NB8): 6817-6828.

Bethke, C. M. (1986). "Hydrologic constraints on the genesis of the upper mississippi valley mineral district from Illinois basin brines." Economic Geology **81**(2): 233-249.

Bethke, C. M. and S. Marshak (1990). "Brine migrations across north-america - the plate-tectonics of groundwater." Annual Review of Earth and Planetary Sciences **18**: 287-315.

Bethke, C. M., J. D. Pruitt, et al. (1984). "Petrographic, geochemical, and paleohydrologic evidence of nature of petroleum migration in Illinois basin." Aapg Bulletin-American Association of Petroleum Geologists **68**(4): 454-454.

Bethke, C. M., J. D. Reed, et al. (1991). "Long-range petroleum migration in the Illinois basin." Aapg Bulletin-American Association of Petroleum Geologists **75**(5): 925-945.

Boggs, S. (2001). Principles of sedimentology and stratigraphy. Upper Saddle River, New Jersey, Prentice-Hall Inc.

Bowen, B. B., R. Ochoa, et al. (2011). "Depositional and diagenetic variability within the Cambrain Mount Simon Sandstone: Implications for carbon dioxide sequestration." Environmental Geosciences **June 2011**: *in press*.

Bredehoeft, J. D., C. R. Blyth, et al. (1963). "Possible mechanism for concentration of brines in subsurface fromations." Bulletin of the american association of petroleum geologists **47**(2): 257-269.

Buschbach, T. C., Ed. (1975). Handbook of Illinois Stratigraphy. Urbana, Illinois State Geological Survey.

Buschbach, T. C. and D. R. Kolata, Eds. (1991). Regional Setting of Illinois Basin. Interior Cratonic Basins, American Association of Petroleum Geologists Memoir.

Carpenter, A. B., Ed. (1978). Origin and chemical evolution of brines in sedimentary basins. Thirteenth annual forum on the geology of industrial minerals, Oklahoma Geological Survey.

Clark, I. and P. Fritz (1997). Environmental isotopes in hydrogeology. New York, CRC Press LLC.

Clayton, R. N., I. Friedman, et al. (1966). "Origin of saline formation waters .1. Isotopic composition." Journal of Geophysical Research **71**(16): 3869-&.

DOE (2010). "Carbon sequestration atlas of the United States and Canada." http://www.netl.doe.gov/technologies/carbon_seq/refshelf/atlasIII/.

Driese, S. G., C. W. Byers, et al. (1981). "Tidal deposition in the basal Upper Cambrian Mt. Simon Formation in Wisconsin." Journal of Sedimentary Research **51**(2): 367-381.

Duffin, M. E., M. C. Lee, et al. (1989). "Potassic diagenesis of Cambrian sandstones and Precambrian granitic basement in UPH-3 deep hole, upper mississippi valley, USA " Journal of Sedimentary Petrology **59**(5): 848-861.

Egeberg, P. K. and P. Aagaard (1989). "Origin and evolution of formation waters from oil fields on the Norwegian shelf." Applied Geochemistry **4**(2): 131-142.
Fishman, N. S. (1997). "Basin-wide fluid movement in a cambrian paleoaquifer: Evidence from the Mt. Simon Sandstone, Illinois and Indiana." Society for Sedimentary Geology Special Publications **57**.
Fouke, B. W., A. J. W. Everts, et al., Eds. (1996). Subaerial exposure unconformities in the Vercors carbonate platform (SE France) and their sequence-stratigraphic significance. High-resolution sequence stratigraphy, Geological Society of London, Special Publication.
Fouke, B. W. and J. Rakovan (2001). "An Integrated Cathodoluminescence Video-Capture Microsampling System." Journal of Sedimentary Research **71**(3): 509-513.
Fouke, B. W., W. Schlager, et al. (2005). "Basin-to-platform chemostratigraphy and diagenesis of the Early Cretaceous Vercors Carbonate Platform, SE France." Sedimentary Geology **175**(1-4): 297-314.
Goetz, L. K., J. G. Tyler, et al. (1992). "Deep gas play probed along rough creek graben in Kentucky part of southern Illinois basin." Oil & Gas Journal **90**(38): 97-101.
Goetze, J., M. Ploetze, et al. (1999). "Defect structure and luminescence behaviour of agate; results of electron paramagnetic resonance (EPR) and cathodoluminescence (CL) studies." Mineral Mag **63**(2): 149-163.
Götze, J., D. Habermann, et al. (1999). "High-resolution spectrometric analysis of rare earth elements-activated cathodoluminescence in feldspar minerals." Chemical Geology **153**(1-4): 81-91.
Götze, J., M. Plötze, et al. (2001). "Origin, spectral characteristics and practical applications of the cathodoluminescence (CL) of quartz – a review." Mineralogy and Petrology **71**(3): 225-250.
Holser, W., Ed. (1979). Trace elements and isotopes in evaporites. Marine Minerals: Reviews in Mineralogy, Mineralogical Society of America.
Houseknecht, D. W. and F. G. Ethridge (1978). "Depositional history of the Lamotte Sandstone of southeastern Missouri." Journal of Sedimentary Research **48**(2): 575-586.
Kolata, D. R., Ed. (1991). Overview of Sequences. Interior Cratonic Basins, American Association of Petroleum Geologists Memoir.
Kolata, D. R., Ed. (2010). Cambrian and Ordovician Systems. Geology of Illinois, Illinois State Geological Survey.
Kolata, D. R. and J. W. Nelson, Eds. (1991). Tectonic History of the Illinois Basin. Interior Cratonic Basins, American Association of Petroleum Geologists Memoir.
Kolata, D. R. and J. W. Nelson, Eds. (2010). Tectonic History. Geology of Illinois, Illinois State Geological Survey.
Land, L. S. and D. R. Prezbindowski (1981). "The origin and evolution of saline formation water, Lower Cretaceous carbonates, south-central Texas, U.S.A." Journal of Hydrology **54**(1-3): 51-74.
Leach, D. L. and E. L. Rowan (1986). "Genetic link between Ouachita foldbelt tectonism and the mississippi valley-type lead-zinc deposits of the Ozarks." Geology **14**(11): 931-935.
Leetaru, H. E., S. Frailey, et al., Eds. (2009). Carbon Sequestration in the Mt. Simon Sandstone Saline Reservoir. Carbon dioxide sequestration in geological media - State of the science, AAPG Studies in Geology.

Leetaru, H. E. and J. H. McBride (2009). "Reservoir uncertainty, Precambrian topography, and carbon sequestration in the Mt. Simon Sandstone, Illinois Basin." Environmental Geosciences **16**(4): 235-243.
Makowitz, A., R. H. Lander, et al. (2006). "Diagenetic modeling to assess the relative timing of quartz cementation and brittle grain process during compaction." Aapg Bulletin **90**(6): 873-885.
Mariano, A. N., J. Ito, et al. (1973). Cathodoluminescene of plagiocalse feldspars. Abstracts with Programs. Boulder, CO, Geological Society of America. **5**.
Marshall, D. J. (1988). Cathodoluminescence of Geological Materials. London, Unwin Hyman.
McBride, E. F. (1989). "Quartz cement in sandstones: a review." Earth-Science Reviews **26**: 69-112.
McBride, J. H., D. R. Kolata, et al. (2003). "Geophysical constraints on understanding the origin of the Illinois basin and its underlying crust." Tectonophysics **363**(1-2): 45-78.
McCaffrey, M. A., B. Lazar, et al. (1987). "The evaporation path of seawater and the coprecipitation of Br (super -) and K (super +) with halite." Journal of Sedimentary Research **57**(5): 928-937.
McKerrow, W. S., C. R. Scotese, et al. (1992). "Early Cambrian continental reconstructions." Journal of the Geological Society **149**(4): 599-606.
Morse, D. G. and H. E. Leetaru (2003). Reservoir Characterization and 3D Models of Mt. Simon Gas Storage Fields in the Illinois Basin. Champaign, IL, Illinois State Geological Survey.
Oliver, J. (1986). "Fluids expelled tectonically from orogenic belts - Their role in hydrocarbon migration and other geologic phenomena - Reply." Geology **14**(12): 1042-1043.
Phelps, T. J. and J. K. Fredrickson, Eds. (2002). Drilling, coring, and sampling subsurface environments. Manual of Environmental Microbiology. Washington, DC, American Society for Microbiology.
Ramm, M. and K. Bjorlykke (1994). "Porosity/depth trends in reservoir sandstones; assessing the quantitative effects of varying pore-pressure, temperature history and mineralogy, Norwegian Shelf data." Clay Minerals **29**(4): 475-490.
Riley, J. P. and R. Chester (1971). Introduction to Marine Chemistry. London and New York, Academic Press.
Rowan, E. L. and G. de Marsily (2001). "Infiltration of Late Palaeozoic evaporative brines in the Reelfoot rift: a possible salt source for Illinois basin formation waters and MVT mineralizing fluids." Petroleum Geoscience **7**(3): 269-279.
Rowan, E. L., M. B. Goldhaber, et al. (2002). "Regional fluid flow as a factor in the thermal history of the Illinois basin: Constraints from fluid inclusions and the maturity of Pennsylvanian coals." Aapg Bulletin **86**(2): 257-277.
Seyler, B. and R. M. Cluff, Eds. (1991). Petroleum Traps in the Illinois Basin. Interior Cratonic Basins.
Siegel, D. I. (1989). "Geochemistry of the Cambrian-Ordovician aquifer system in the northern Midwest, United States." Journal Name: United States Geological Survey, Professional Paper; (USA); Journal Volume: 1405-D: Medium: X; Size: Pages: D1-D76.
Sippel, R. F. (1968). "Sandstone petrology, evidence from luminescence petrography." Journal of Sedimentary Research **38**(2): 530-554.
Sloss, L. L. (1963). "Sequences in the cratonic interior of North-America." Geological Society of America Bulletin **74**(2): 93-93.

Stueber, A. M., P. Pushkar, et al. (1987). "A strontium isotopic study of formation waters from the Illinois basin, U.S.A." Applied Geochemistry **2**(5-6): 477-494.
Stueber, A. M. and L. M. Walter (1991). "Origin and chemical evolution of formation waters from Silurian-Devonian strata in the Illinois basin, USA." Geochimica Et Cosmochimica Acta **55**(1): 309-325.
Stueber, A. M., L. M. Walter, et al. (1993). "Formation waters from Mississippian-Pennsylvanian reservoirs, Illinois basin, USA: Chemical and isotopic constraints on evolution and migration." Geochimica Et Cosmochimica Acta **57**(4): 763-784.
Taylor, J. M. (1950). "Pore-space reduction in sandstones." Bulletin of the american association of petroleum geologists **34**(4): 701-716.
Thompson, A., Ed. (1959). Pressure solution and porosity. Silica in sediments, Society of Economic Paleontologists and Mineralogists Special Publication.
Trewin, N. H. and A. E. Fallick (2009). Quartz Cement Origins and Budget in the Tumblagooda Sandstone, Western Australia, Blackwell Publishing Ltd.
Treworgy, J. D., S. T. Whitaker, et al. (1997). Structural cross section of the Paleozoic rocks in Illinois, Wayne County to Stephenson County.
Veizer, J., D. Ala, et al. (1999). "Sr-87/Sr-86, delta C-13 and delta O-18 evolution of Phanerozoic seawater." Chemical Geology **161**: 59-88.
Visocky, A. P., M. G. Sherrill, et al. (1985). Geology, hydrology, and water quality of the Cambrian and Ordovician systems in northern Illinois. Champaign, Ill., State of Illinois, Dept. of Energy and Natural Resources.
Walter, L. M., A. M. Stueber, et al. (1990). "Br-Cl-Na systematics in Illinois basin fluids - Constraints on fluid origin and evolution." Geology **18**(4): 315-318.
Weibel, R., H. Friis, et al. (2010). "Development of early diagenetic silica and quartz morphologies -- Examples from the Siri Canyon, Danish North Sea." Sedimentary Geology **228**(3-4): 151-170.
Worden, R. H. and S. Morad, Eds. (2000). Quartz cementation in oil field sandstones: a review of the key controversies. Quartz Cementation in Sandstones, Blackwell Science.